1 Polar nephelometers for light scattering by ice crystals and aerosols: design and measurements

Brian Barkey, Suzanne Paulson and Kuo-Nan Liou

1.1 Introduction

The angular distribution of light scattered from a particle is dependent on its size, shape, composition and on the wavelength and polarization state of the incident light. This information is of tremendous interest to many researchers due to implications in the fields of remote sensing, climatic effects of radiative transfer, and in industrial and scientific laboratories in applications such as aerosol monitoring (Hansen and Lacis 1990; Liou et al. 1999; Mishchenko et al. 1995). The measured angular scattering patterns can lend insights into the chemical and physical properties of the particles (i.e., Pluchino 1987; Swanson et al. 1999; Shaw 1979). The interest in these data is shown by the over 25 polar nephelometers (PN) described in this chapter, that have been built since the 1960s to experimentally examine the angular scattering properties of various small particles. The goals of these measurements are either to verify the increasingly complex theoretical methods of calculating the scattering properties of non-spherical particles, or to use the angular intensities to infer optical, physical or chemical properties of the particles.

The scattering angle (θ) is referenced from the direction of the incident light as shown in Fig. 1.1 with $\theta = 0^\circ$ coincident with the incident light vector and $\theta = 180^\circ$ is the direction towards the light source. The azimuthal angle (ϕ) is defined from an arbitrary axis oriented in the plane perpendicular to the incident light direction and ranges from 0° to 360°. The angular distribution of light intensities from a randomly oriented particle is generally a function of both θ and ϕ.

Theoretically, there are many ways in which to calculate the light scattering properties of particles, or phase functions, including homogeneous spheres (Mie 1908), coated spheres (Aden and Kerker 1951), and other non-spherical shapes (Mishchenko 1991; Takano and Liou 1989; Yang and Liou 1996). Although these models have a strong theoretical basis and are able to capture the scattering properties of very complex morphologies, experimental measurements are necessary because the physical, chemical and optical properties of the scattering particles are largely unknown. For instance, measured and inferred refractive indices for several types of black carbon based aerosols range from 1.1 to 2.75 in the real part and from 0.01 to 1.46 in the imaginary part (Bond et al. 2006; Fuller et al. 1999; Horvath 1993; Seinfeld and Pandis 1998), although the refractive index of pure carbon

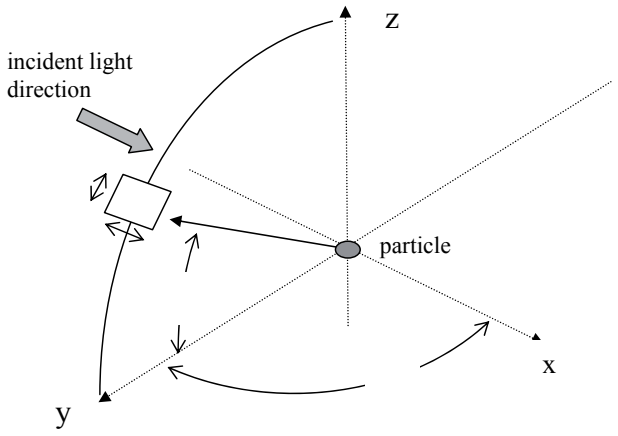

Fig. 1.1. The scattering angle (θ) is referenced from the direction of the incident light. The particle is located at the intersection of the axis. In this figure $\theta = \pi/2$. The azimuthal angle (ϕ) is defined from an arbitrarily defined axis, but is usually referenced to the polarization plane of the incident light if it is linearly polarized.

$(2.67 - i1.34)$ (Borghesi and Guizzetti 1991) is well known. These unknowns can have significant effects on the radiative properties of aerosols. For example, the asymmetry parameter, which is the cosine-weighted integral of the light scattered from a particle, is a key parameter in radiative transfer models. The asymmetry parameter varies by a factor of at least 10 as the number of agglomerated spherules changes from 1 to 200 (Liu and Mishchenko 2005). Cirrus clouds are composed of ice particles with highly complex shapes that vary significantly in space and time which affects their single scattering and bulk radiative properties. The theoretically determined asymmetry parameter can vary from 0.77 to 0.84 at a wavelength of 0.55 μm for simple hexagonal ice particle morphologies and distributions seen in nature (Takano and Liou 1989). However measured values of the asymmetry parameter for low-latitude cirrus clouds range from 0.74 to 0.77 (Garrett et al. 2003). An increase in g of 0.06 was shown to cause a decrease in radiative forcing by at least 12% for non-absorbing particles (Marshall et al. 1995). Accurate and reliable morphologically based scattering information for these particles is necessary as cirrus clouds contribute significantly to the earth's radiative balance (Liou 1986).

In concept, polar nephelometers are simple instruments. A particle is illuminated with a highly collimated beam of light, most often from a laser, and a detector (or detectors) measure the light intensities at the desired angles. But, complexities arise in the detection geometry, sample presentation and in the analysis of the measurements. This chapter presents a review of some of the designs of polar nephelometers, and presents a short summary of the measurements made, including our previous ice particle and aerosol studies. Finally, we describe the current dual polarization polar nephelometer (UCLA PN) developed at UCLA, non-absorbing and absorbing aerosol particle scattering measurements, and a detailed analysis of the refractive index retrieval accuracy.

1.2 Measuring the intensity of scattered light

Measuring the angular dependence of light scattered by a particle is done by placing a detector at the proper angular location with respect to the incident light and determining the intensity of the light that falls onto the detector's sensing area. In practice, however, there are many complications to the experimental setup, i.e.: How many particles are scattering light? What volume do the particles occupy? What is the orientation of the particles? Detectors have finite sensing areas, how wide is it? And so on. In this section, a few of these questions are addressed; however, it should be realized that due to the many possible instrument designs, a complete analysis of all polar nephelometer design considerations cannot be included.

1.2.1 Geometry

The direction of light scattered from a particle is defined by the scattering (or polar) angle (θ) and the azimuthal angle (ϕ) as shown in Fig. 1.1. The azimuthal reference angle or $\phi = 0°$ is arbitrarily defined, however, if the incident light has a preferred polarization orientation, this direction often defines the $\phi = 0°$ direction. θ and ϕ thus defined represent all the directions in the space about the particle. It is impossible to measure the scattering at 0° and 180° as the light scattered at $\theta = 0°$ cannot be separated from the incident light, and any detector positioned at the reverse angle of $\theta = 180°$ would obscure the incident beam. The instruments reviewed in this paper measure the light scattered from particles with relevance to atmospheric radiative transfer, such as aerosols, cloud water drops and cirrus cloud particles. These particles usually have maximum dimensions smaller than 1 to 100 μm and thus are usually randomly oriented when suspended in air. Perrin (1942) used symmetry relationships to show that there is no azimuthal dependence to the light scattering from a small volume of randomly oriented particles when the incident light is not polarized. There are situations in which these symmetry relations do not hold, such as for larger ice particles which have preferred orientations when falling (Klett 1995).

Detectors have a finite field of view defined in Fig. 1.1 as the area inside the box with width $\Delta\theta$ and $\Delta\phi$. Here, the detector's field of view is rectangular, but detection apertures can be circular, slits or other shapes. Unless the scattering is from a single particle, light is scattered from a volume containing several particles which is defined by the either the field of view of the detector (which is often defined by collection optics on the detector) and/or the volume of particles illuminated by the incident light (i.e., a stream of particles that intersect the laser beam). In general, for linearly polarized incident light, the measured scattered intensity, $I(\theta_i)$, is

$$I(\theta_i) = \frac{\lambda^2}{4\pi^2} \int_{\theta_1}^{\theta_2} \int_{\phi_1}^{\phi_2} \left(I_1(\theta,\phi) + I_2(\theta,\phi)\right) k(\theta,\phi)\, \sin\theta \, d\theta \, d\phi \qquad (1)$$

where λ is the wavelength of the incident light, $k(\theta,\phi)$, defines the detector response to light scattered into the angle θ and ϕ, and is a function of the sensing geometry, the scattering volume and the detector response properties. $I_1(\theta,\phi)$ and $I_2(\theta,\phi)$ are the light intensities scattered parallel and perpendicular to the reference plane

and are dependent on the polarization direction of the incident light, the refractive index (m) of the scattering particles and the number, shape and size of particles in the scattering volume. For randomly oriented or symmetric particles with non-polarized incident light, the azimuthal dependence can be ignored (Van de Hulst 1957; Perrin 1942). For detectors with a narrow angular field of view, detector surface response characteristics introduce very small errors (Jones et al. 1994).

Determining the response characteristics of a polar nephelometer depends on the geometry of each design and usually requires three-dimensional numerical integration across the various scattering and sensing angles. An example is shown in Fig. 1.2(a) which is a top view of the UCLA polar nephelometer showing the sensing geometry of two detector positions. Variables are described in Table 1.1.

Table 1.1. Parameters/descriptions for selected figures.

Figure	Variable	Definition
2(a)	$D_L, -D_L$	Extent of particle volume which is defined by the sample guide tubes.
	a_l	Position of a particle on the line defined by the laser beam.
	R_d	Distance from the center of the scattering plane to the detector.
	r_d	Detector radius
	θ_i	Angular position of the detector at channel i.
	θ	Scattering angle of the photon that origines from the particle at position a_l and that lands on the detector at a position a_d.
Figure	Variable	Description
4(a)	⧫	Experiment: Irregular ice particles, $T = -41^\circ$C, mean maximum dimension $= 7.5\,\mu$m. Theory: Randomly oriented bullet rosettes and plate crystals calculated using the unified theory of light scattering by ice crystals (Liou et al. 1999)
	□	Experiment: water droplets, mean diameter $= 7.5\,\mu$m. Theory: Mie–Lorentz, mean diameter $= 7.5\,\mu$m, standard deviation $= 0.2\,\mu$m, refractive index $= 1.33 - i0.0$.
4(b)	▲	Experiment: Growth $T \cong -6^\circ$C. Mean maximum dimension $= 36 \pm 0.5\,\mu$m. Theory: based on the observed hollow column and short column habits with rough surfaces on 80% of the particles, calculated using geometric ray-tracing (Takano and Liou 1989).
4(c)	⧫	Experiment: Growth $T < -10^\circ$C. Mean maximum dimension $= 17 \pm 0.5\,\mu$m. Theory: based on the observed short column and plate habits with rough surfaces on 80% of the particles, calculated using geometric ray-tracing (Takano and Liou 1989).
7	⧫, •	Experiment: Ammonium sulfate $(NH_4)_2SO_4$-H_20 droplets. Incident light polarized parallel (⧫) and perpendicular (•) to the scattering plane. Theory: Mie–Lorentz, mean diameter $= 60$ nm. GA determined $m = 1.414 - i0.0$.

More information on this instrument is given in section 1.4 and Fig. 1.6. In this instrument the particles are confined to the center of the scattering volume via a sample guide tube with a rectangular cross-section in a swath about 19 mm long and 4 mm wide, parallel and coincident with the laser beam. To simplify this anal-

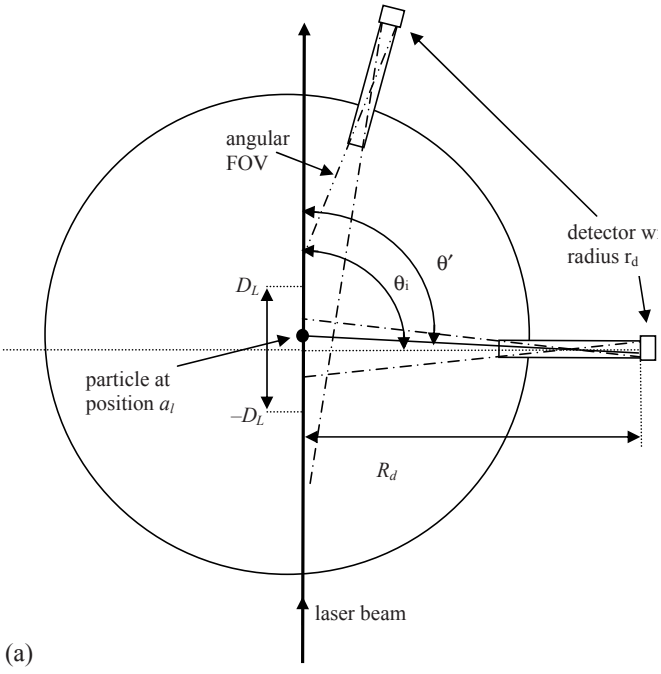

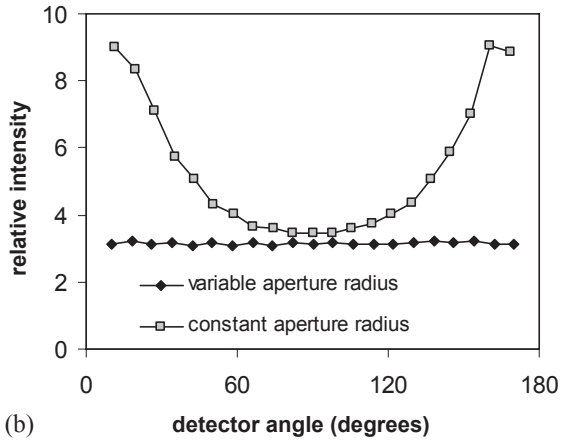

Fig. 1.2. (a) Top view of the UCLA polar nephelometer showing two detector positions to detail dimensions relevant to calculating the scattering response. Particles intersect the incident laser beam in the rectangle at the center of the scattering array. Definitions of the variables are in the text and in Table 1.1. (b) The UCLA polar nephelometer relative response to particles that scatter isotropically with detector apertures that are equal in size and with apertures sizes adjusted to remove the non-uniform response.

ysis, particles are assumed to lie on the laser beam line which is reasonable as the laser beam width is about 1 mm and the azimuthal scattering dependence is ignored as the maximum azimuthal sensor extent is only 3° above and below the scattering plane. Each detector has a finite area, defined by its radius r_d. The scattering angle, θ', for a particle located between $-D_L$ and D_L that scatters a photon that falls at a location between $-r_d$ and $+r_d$ on the detector is not usually the same as the angular position of the detector θ_i as shown in Fig. 1.2. The relative intensity, $I_r(\theta_i)$, of light scattered into each channel i is determined via;

$$I_r(\theta_i) = C_i \int_{a_l=-D_L}^{a_l=D_L} \int_{a_d=-r_d}^{a_d=r_d} I_p(\theta'(a_l, a_d)) \left(\frac{R_d}{R'(a_d, a_l, \theta_i)} \right)^2 D(\theta', a_d, a_l)\, da_d\, da_l \quad (2)$$

where the integral is for all the particle positions along the laser beam from $a_l = +D_L$ to $-D_L$ and from all the scattered photon landing positions on the detector between $a_d = -r_d$ to $+r_d$. Due to inherent differences in detector gain, a calibration constant C_i is applied and discussed in more detail in section 1.4.3.1 and eq. (7). The intensity of the light scattered into the angle θ for the types and distribution of particles is denoted by $I_p(\theta(a_l, a_d))$ where the subscript 'p' indicates that the incident light is polarized parallel or perpendicular to the measurement plane. From simple geometry θ is a function of the position of the particle (a_l) and where its photon lands on the detector (a_d) via;

$$\theta'(a_l, a_d) = \tan^{-1} \left[\frac{a_l \cos\theta_i + R_d}{a_l \sin\theta_i - a_d} \right] \quad (3)$$

where R_d is the detector's distance from the center of the scattering plane. Because the distance between the particle location a_l and where its photon lands on the detector at a_d is not the same as R_d, the scattered intensity is adjusted by the second term in the integral of eq. (2) where;

$$R'(a_d, a_l, \theta_i) = \left[(a_l \sin\theta_i - a_d)^2 + (a_l \cos\theta_i + R_d)^2 \right]^{\frac{1}{2}}. \quad (4)$$

$D(\theta',\ a_d,\ a_l)$, which is not explicitly defined here, accounts for the circular shape of the detector aperture as the amount of light getting to the detector is dependent on the height of the hole where the photon enters the aperture.

In this design, the scattering volume is rectangular in order to maximize the number of particles scattering light into the angles near 90° as the intensities at this angle are usually much lower than those in the forward directions. However, because of this, much more light is detected in the forward and reverse directions as shown in Fig. 1.2(b) as the plot marked 'constant aperture radius' in which the relative response for a particle which scatters isotropically is calculated as discussed above with a constant aperture diameter of 4.75 mm. The larger forward response limits the instrument in that the dynamic range of the instrument is reduced, i.e., the intensities at the forward and reverse angles cause the detectors to saturate at relatively low particle concentrations, and also post-processing of the measured signal is required in order to compare measured response to theoretical results. To reduce this problem, the aperture diameters in the newest UCLA nephelometer

have diameters which range from about 3 mm in the forward and reverse directions and increase to about 4.7 mm at the side scattering angles. Thus, the response to an isotropic source is more constant as shown by the plot labeled 'variable aperture radius' in Fig. 1.2(b).

1.2.2 Beam considerations

The intensity of the light across a laser beam is not constant, and for Gaussian TEM_{00} (single mode lasers) the radial intensity profile of the laser beam is described by $I(r) = I_{c0} \exp(-2r^2/w^4)$, where $I(r)$ is the intensity of the laser light at the beam radius r, I_{c0} is the laser beam intensity at the center of the laser beam, and w is the laser beam waist, or the laser beam radius at which the laser beam intensity falls to a value $1/e^2$ of the axial value. Colak et al. (1979) has shown that for a sphere if the beam waist is 5 times greater than the particle maximum dimension, then differences between the light scattered by the Gaussian beam and that by a plane wave differ by less than 5%. Small deviations in the collimation of the light source do not affect the scattered intensities greatly unless the beam size is comparable to the size of the particle (Barkey et al. 1999).

The overall sensitivity of the instrument is proportional to the intensity of the incident beam. However, it is possible to 'burn' the particles, which can cause erroneous measurements. The maximum amount of power is a function of the type of particle studied, i.e., particles which absorb very little can tolerate much more incident light, the wavelength of the light, the beam profile and size and the amount of time the particle spends in the beam (Lushnikov and Negin 1993). A convenient upper limit is 210 W/cm^2 as this intensity will cause 150 μm diameter carbon particles, which are the most absorptive particles likely to be encountered, to ignite in 7 milliseconds in a 1 μm wavelength laser beam (Bukatyi et al. 1983).

1.2.3 Stray light

Detectors in polar nephelometers monitor the light scattered into a small fraction of the full 4π solid angle about the sample. Particles however scatter light into the full 4π solid angle and this light needs to be handled. The intensity of light scattered into the near forward angles is orders of magnitude higher than that scattered into the side and reverse directions. If only a small percentage of this light undergoes multiple internal reflections within the working volume of the instrument it can 'leak' to the detectors and a effect the measurement. Common methods to reduce stray light includes blackening the interior surfaces of the instrument and designing optics or apertures (discussed above in section 1.2.1), to restrict the detectors' field of view. A beam dump to collect the light exiting the scattering volume is necessary to prevent the incident light from scattering back into the measurement volume. We have found that a properly designed 'Rayleigh' horn beam dump is much more effective than the stacked razor-blade style.

In the multi-detector design of the UCLA polar nephelometer, all surfaces in direct view of the sample volume and the detectors are polished and angled such that scattered light is directed away from the detection plane. The large area photodiode detectors in this instrument are also effective reflective surfaces, hence the

detectors are positioned such that each detector is not in the field of view of another detector. For example, for the detector at 10°, a detector is not also placed directly across the scattering plane at the position of 100°.

1.3 Polar nephelometer designs and some measurements

There are many different designs of instruments that measure the angular scattering properties of particles. The discussion here is limited to those instruments that have small angular resolutions, i.e. their detector(s) span only about 1° to 2° of the scattering angles. Instruments that have wider angular detection limits, i.e., greater than 45°, and which approximate the measurement of integrating nephelometers are not considered (Szymanski et al. 2002). There are also instruments that measure the scattering properties in the microwave region (Chỳlek et al. 1988; Zerull et al. 1977; Zerull et al. 1980) but these are not considered as this review is limited to measurements in the visible and infrared wavelengths. Although the optical equivalence theorem allows us to apply results from this measurement to smaller wavelengths, microwave experiments face the problem of constructing equivalently sized particles that are truly analogous to the aerosol, dust or ice particles of interest in the visible and infrared regions.

A few instruments isolate a single particle in an electromagnetic field (Bacon and Swanson 2000; Bacon et al. 1998; Pluchino 1987) but most polar nephelometer designs measure the light scattered from a narrow stream of particles intersecting a collimated light beam. As such, they are not strictly single scattering measurements as they measure the light scattered from many particles in a small volume. However, if the average distance between each particle is large compared to the average particle size, and the wavelength and the scattering volume is small compared to the detector-to-sample distance, then single scattering can be assumed (Mishchenko et al. 2004). A few instruments (Castagner and Bigio, 2006, 2007; Schnaiter and Wurm, 2002) isolate the sample in a glass tube; however, interaction of the scattered light with the container material can potentially introduce errors.

Polar nephelometers can be categorized broadly according to their sensing geometry, illustrated in Fig. 1.3. Designs include goniometer instruments (Fig. 1.3(a)), multi-detector devices (Fig. 1.3(b)) and elliptical mirror (Fig. 1.3(c)) devices. This last category describes instruments that use elliptical mirrors to redirect the scattered light to intensity detectors in a manner such that the scattering angle information is preserved.

1.3.1 Goniometer-type polar nephelometers

Shown in Table 1.2 is a compilation of several polar nephelometers that rotate a detector (or detectors) to the desired angular position. These instruments have the advantage of high angular resolution as the detector can be stepped at any desired angular increment. This process does have the drawback of requiring more time to measure all of the desired angles. Thus the sample stream needs to be maintained at a constant concentration for a relatively long period of time. Methods are available to correct for variations in the particle concentration (i.e., Sassen and Liou

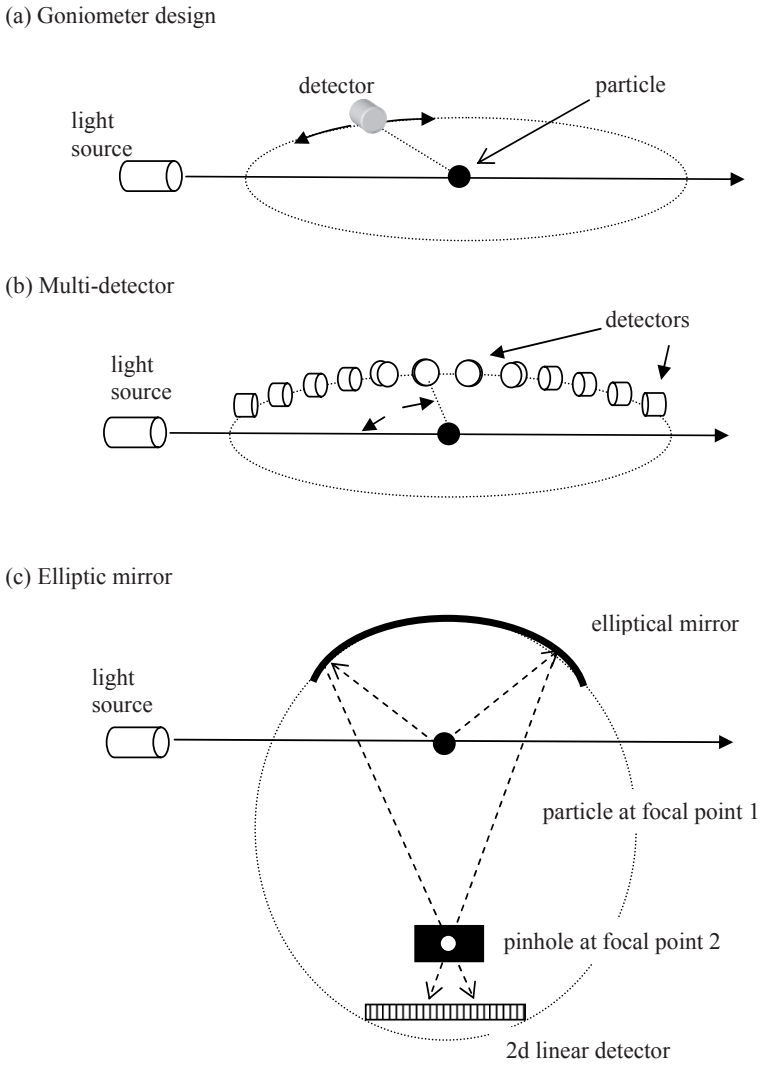

Fig. 1.3. (a) Goniometer type nephelometer geometry. A few detectors (1–3 usually) are mounted on a gimbal device that allows the detector to move to the selected scattering angle. (b) Multi-detector geometry in which several detectors are fixed at discrete angular positions. (c) In the elliptical mirror configuration, an elliptical mirror is used to focus the scattered light onto a linear detection array (or a 3D array in which 2D information is derived). The pinhole prevents light scattered from undesirable angles from getting to the sensor.

1979a) by using a separate fixed-angle detector to monitor sample concentration consistency.

Because there is only one detector, several goniometer instruments have the capability to measure the Mueller matrix. The Mueller matrix describes completely how the polarization properties of the scattered light are affected by the particles and has implications in remote sensing (Ou et al. 2005) and in the inversion of par-

Table 1.2. Compilation of polar nephelometers based on the goniometer design.

Light source	Measured polarization quantity	Angular extent	Particles	Reference
496 nm 552 nm 630 nm	Mueller matrix via rotating compensator	10°–170°	Fogs, light rain	Gorchakov 1966
Various visible	Unpolarized intensity	∼ 5°–175°	Talc powder	Holland and Draper 1967
486 nm 546 nm	Mueller matrix via difference method	18°–166°	Crystalline silica (sand)	Holland and Gagne 1970
475 nm 515 nm 745 nm	I^{**}_{parallel} $I^{**}_{\text{perpendicular}}$	∼5°–175°	Ice crystals	Huffman 1970
632.8 nm 325 nm	Mueller matrix via electro-optical polarization modulator	∼30°–160°	NaCl crystals, Ammonium sulfate spheres	Perry et al. 1978
632.8 nm	Intensity, DLP*	10°–165°	Water, ice crystals, mixed phase	Sassen and Liou 1979a; 1979b
408 nm 450 nm 570 nm 546 nm 578 nm	Mueller matrix elements via difference method	∼5°–180°	Water, ice clouds	Dugin et al. 1971; Dugin and Mirumyants 1976; Dugin et al. 1977
514.5 nm	Mueller matrix via difference method	2°–178°	N_2, ambient aerosols	Hansen and Evans 1980
514.5 nm	Intensity, DLP*	7°–170°	Ambient aerosols	Tanaka et al. 1983
532 nm	Mueller matrix via electro-optical polarization modulator	∼11°–170°	Marine boundary area like aerosols	Quinby-Hunt et al. 1997
632.8 nm	Selected Mueller matrix elements	4°–170°	N2 gas, ambient aerosols	Zhao 1999
632.8 nm 441.6 nm	Mueller matrix via electro-optical polarization modulator	3°–174°	Various mineral dusts	Volten et al. 2001
680 nm	Intensity, DLP*	∼ 30°–155°	PSL with various agglomerations	Schnaiter and Wurm 2002
441.6 nm, 632.8 nm	Mueller matrix via electro-optical polarization modulator	3°–174°	Water, quartz dust	Kuik et al. 1991 Hovenier et al. 2003
532 nm	$I^{**}_{\text{perpendicular}}$	2°–178°	Ambient aerosols	Lienert et al. 2003

* Degree of linear polarization.
** Incident or measured light polarized parallel or perpendicular to the scattering plane.

ticle properties (Zhao 1999; Kuik et al. 1991; Quinby-Hunt et al. 1997). Gorchakov (1966) rotated a mica compensator placed at the exit of the incident light and used tuned amplifiers at the photomultiplier detector to select various harmonics from the scattered light to determine the Mueller matrix elements. The matrix elements can also be measured via the phase-sensitive detection of various components of the scattered light in which the polarization of the incident light is time modulated as described by Hunt and Huffman (1973). These polarization-sensitive instruments have been used for measurements of various mineral aerosols that can be aerosolized by mechanical means (Hovenier et al. 2003) or nebulized in an aqueous solution and then dried (Perry et al. 1978). Mueller matrix elements have been measured for ice crystals (Dugin et al. 1971; Dugin and Mirumyants 1976; Dugin et al. 1977), but using the less accurate and more time-consuming difference method (Liou 1975), in which various polarization elements are placed in front of the source and detectors. Measurement errors inherent in this approach are significant as derivation of the Mueller matrix elements requires the determination of small differences between large values. The goniometer instrument developed by (Zhao 1999) was specifically designed to derive only a few of the Mueller matrix elements in order to determine the refractive index of aerosols via inversion of the Mie–Lorenz solution for scattering from a homogeneous sphere.

1.3.2 Multi-detector polar nephelometers

Table 1.3 lists instruments in which several detectors are placed at discrete and fixed angular locations as shown in Fig. 1.3(b). The design by West et al. (1997) uses 6 linear detector arrays that measure the intensity of light scattered into 6 angular swathes defined by focusing optics. Pluchino (1987) isolates a single particle in an electric field and uses fiber-optic light guides to direct scattered light to photodiode detectors. These instruments have simpler designs and the advantage that they can make fast (real-time) measurements. This is particularly desirable for measuring the time evolution of scattering properties, which can provide insights into particle growth or decay properties. The multi-detector designs are also relatively easy to ruggedize and thus suitable for measurements in the field and in more demanding laboratory environmental conditions. Because the response characteristics between each detector are different, calibration is required. Due to the complexity and expense of providing analyzing optics at each channel none of these instruments measure the polarization state of the scattered light. In a nephelometer design by Dick et al. (2007), along with scattering measurements between $\theta = 40^\circ$ to 140° there are eight detectors at various azimuthal angles at $\theta = 55^\circ$. These azimuthal detectors ensure that only scattering from spherical particles is recorded as the scattering from spherical particles with unpolarized incident light is not azimuthally dependent.

1.3.3 Elliptical mirror polar nephelometers

Table 1.4 lists several instruments that are based on the measurement of scattered light that is redirected by an ellipsoidal mirror to a detector as shown in Fig. 1.3(c). Elliptic mirrors have two focal points, thus light scattered at one focal point will be

Table 1.3. Compilation of multi-channel polar nephelometers.

Light source	Measured polarization quantity	Angular extent	Particles	Reference
855 nm	Intensity	23.1°–128.3°	Gases, PSL spheres, Ambient aerosols	Leong et al. 1995
1064 nm	Intensity	5°–175°	Evaporating water drops and ice crystals	Pluchino 1987
804 nm	Intensity	3°–169°	Ice crystals	Gayet et al. 1998
488 nm	Intensity	40°–140°	Aerosols	Dick et al. 1998; 2007
670 nm	$I^{**}_{\text{perpendicular}}$	5°–175°	Ice crystals	Barkey and Liou 2001; Barkey et al. 2002
670 nm	I^{**}_{parallel} $I^{**}_{\text{perpendicular}}$	5°–175°	PSL spheres, ammonium sulfate	Barkey et al. 2007
840 nm	Intensity	23°–129°	Freon-12, PSL spheres for refractive index inversion	Jones et al. 1994
470 nm 652 nm 937 nm	Intensity, DLP*	15°–170°	Mineral dusts	West et al. 1997

* Degree of linear polarization.
** Incident or measured light polarized parallel or perpendicular to the scattering plane.

focused onto the other focal point. A linear array detector placed just beyond the second focal point can thus derive the angular scattering information as a direct correlation exists between the scattered angle and the position the scattered light falls on the detector. In the instrument devised by Kaye et al. (1992) and Hirst et al. (1994) the light scattered between about 30° and 141° and all of the azimuthal angles are measured simultaneously by focusing them onto a two-dimensional detection array. The degree of linear polarization is determined by selecting the measured intensities parallel or perpendicular to the polarization plane of the incident light. Castagner and Bigio (2006; 2007) use a clever arrangement of two parabolic mirrors and a rotating mirror to scan across the angular scattering directions. To ensure only light focused by the elliptical mirror falls onto the detector, this design requires a slit (or pinhole) at the focal point of the elliptical mirror. The size of this aperture defines the angular resolution of the measurement. The slit also reduces the amount of scattered light reaching the detector. Depending on the response characteristics of the detector, measured voltages must be integrated for a significant period of time (minutes) in order to obtain a clear signal (Curtis et al. 2007). None of the elliptical mirror instruments developed to date derive the Mueller scat-

Table 1.4. Compilation of polar nephelometers that use elliptical mirrors.

Incident wavelength	Measured polarization quantity	Angular extent	Particles	Reference
632.8 nm	$I^{**}_{\text{perpendicular}}$	70°–125°	PSL	Castagner and Bigio 2006; 2007
685 nm	Intensity	10°–160°	Ambient aerosols	Kaller 2004
632.8 nm	Intensity, DLP*	30°–141° all azimuthal angles	PSL, various non-spherical dusts	Kaye et al. 1992; Hirst et al. 1994
550 nm	Intensity, DLP*	19°–175°	PSL, ammonium sulfate, 1uartz dusts	Curtis et al. 2007

* Degree of linear polarization.
** Incident or measured light polarized parallel or perpendicular to the scattering plane.

tering matrix elements. However, it is conceivable that a single analyzing optic can be placed at the secondary focal point to achieve this task.

1.3.4 Calibration

Calibration is necessary to ensure the validity of the measurements of all polar nephelometer designs. In multi-detector polar nephelometer designs there are differences in the response characteristics of each detector resulting from variations inherent in the manufacturing processes. At least four methods have been developed to calibrate scattering responses. Barkey and Liou (2001) and Barkey et al. (2002) used an isotropic light point-source placed at the scattering center to ensure equitable response at all channels. More commonly, spherical scattering particles with known refractive indices and size distributions are used. Non-absorbing polystyrene latex (PSL) microspheres which are available in several mono-disburse sizes have a well characterized refractive index as a function of wavelength. Exact scattering expectations can be developed from the Mie–Lorenz solution as these particles are known to be spherical and homogeneous. A few nephelometers are calibrated using molecular scattering from a gas (Jones et al. 1994; Zhao 1999). Ammonium sulfate and water mixtures can also be aerosolized to form spherical particles and have a well-defined refractive index, which varies somewhat with relative humidity (Tang and Munkelwitz 1991; 1994) and are also used for calibration and verification (Barkey et al. 2007; Curtis et al. 2007).

There is no accepted calibration standard for absorbing particles. Aerosolized and dried nigrosin (or more commonly 'India' ink) is used as a calibration standard by many instruments that measure aerosol absorption (Abo Riziq et al. 2007); however, there is significant variation between the reported refractive indices (Spindler et al. 2007). The uncertainty in these values probably arises from the fact that nigrosin is not manufactured for use as a standard, thus there are slight changes in the formulation from batch to batch. Also there are differences in how the nigrosin is aerosolized and dried.

PSL particles have been infused with various colored dyes, but these are not designed as absorption standards and there are differences in the refractive indices measured by various researchers. Inverting the measured angular scattering properties of black dyed PSL spheres suspended in water, Chae and Lee (1993) found a complex refractive index of $1.569 - i0.0$. Lack et al. (2009) found a refractive index value of $1.60(\pm 0.03) - i0.045(\pm 0.004)$ for aerosolized black dyed spheres using a cavity ring down transmissometer. We have found experimentally (from an unpublished experiment) that the refractive index of 1003 nm in diameter black dyed PSL spheres has a refractive index of $1.73 - i0.11$. The source of the particles used by Chae and Lee (1993) was different than that used by Lack et al. (2009) and by our group. The non-absorbing behavior of the Chae and Lee (1993) particles was attributed to the insensitivity of their scattering apparatus to their particles and the small amount of dye relative to the volume of PSL. We have found that treating the particles as a concentric sphere produced a core refractive index of $1.61 - i0.0054$ and a shell refractive index $= 1.64 - i0.03$. It is believed that the PSL spheres are not homogeneously infused with the dye, which is supported by the similarity between our shell refractive index and that of Lack et al. (2009). Also, Lack et al. (2009) found that the coated-sphere model better explained their results before they requested a special batch of PSL particles that were 'cooked' longer in order to more completely infuse the dye (via personal communication with D. Lack).

1.3.5 Applications

Polar nephelometer measurements are used for a variety of goals. These include experimental verification of existing theoretical methods of calculating single scattering characteristics using particles with well-known properties. They have also been applied to quantify and identify differences between the measured and expected scattering when either the particle morphology or scattering theory is less established. The validity of the Mie–Lorenz scattering solution has been demonstrated repeatedly for spherical and homogeneous particles and provides a method for calibration, as discussed above. In contrast, several studies of non-spherical particles, including mineral dusts, readily confirm that there are differences between the Mie–Lorenz assumption and scattering from non-spherical particles (Curtis et al. 2007; Kuik et al. 1991; Perry et al. 1978; Volten et al. 2001). In this section, we review some of the ice particle and aerosol scattering measurements made by our group.

1.3.5.1 Ice particle measurements

Ice crystals have highly irregular shapes, but the refractive index as a function of wavelength is well known (Warren and Brandt 2008). Predicting the angular scattering properties of hexagonally shaped ice crystals requires computer-intensive algorithms such as ray-tracing (Takano and Liou 1989), finite-difference time-domain (Yang and Liou 1996) or T-matrix methods (Baran et al. 2001). The light scattered from ice particles is very different from that scattered from water droplets. For instance, shown in Fig. 1.4(a) (the plot labeled 'ice measurement') is the 670 nm

unpolarized light scattered from irregular ice particles as measured by a 33-channel polar nephelometer (Barkey and Liou 2001). This polar nephelometer used fiber-optic light guides to couple light from the two-dimensional scattering plane to silicon photodiode detectors. Due to the small diameter of the light guides (2 mm) it was possible to concentrate a few detectors near 22° to study the expected halo features from ice crystals. The ice particles are made from water drops generated in an ultrasonic humidifier that are injected into a dry-ice-cooled cold box with a temperature of about −30°C and has a volume of about 0.5 m^3. The resulting particles have an average maximum dimension of about 7.5 μm and non-spherical shapes, but they do not have the clearly defined hexagonal features normally expected for ice particles, as shown in the photomicrograph of the particles replicated on a slide using the vapor method (Takahashi and Fukuta 1988). It is believed that these smaller, ill-defined particle habits arise because all of the water drops produced by an ultrasonic humidifier are homogeneously nucleated immediately by the stainless steel walls of the cloud chamber, which are in direct contact with the dry ice. The rainbow peak, an intensity feature seen in the reverse direction at about 140° is seen for spherical water drop particles as shown in Fig. 1.4(a), the plot labeled 'water measurement'. The water drops are produced from the same ultrasonic humidifier as the ice particle experiment and also have an average diameter of about 7.5 μm. Not only is the rainbow peak absent from the ice particle measurement, but the ice particle scattering is more isotropic. Although the theoretical expectation for the water drop matches the measurement within the 10% measurement error, the level of agreement for the ice particle comparison is much lower. This is most likely due the difficulty in describing the irregular ice particle shape using randomly oriented bullet rosettes with rough surfaces calculated with the unified theory of light scattering by ice crystals (Liou et al. 1999).

The Desert Research Institute (University of Nevada, Reno) ice particle growth column can produce larger ice crystals with more selectable habits. Cooled water droplets from ultrasonic humidifiers are injected at the top of the column and are homogeneously nucleated by a liquid-nitrogen-cooled wire near the middle of the 4 m tall column. These nucleated particles grow with water vapor supplied by the remaining water drops as the saturation vapor pressure of water over ice is lower than that of water vapor over liquid water. The habit of the particles is largely controlled by the temperature in which they grow (Nakaya 1954). Fig. 1.4(b) shows the measured angular scattering intensities for predominately columnar ice particles, while Fig. 1.4(c) shows the same for particles that are mostly plates (Barkey et al. 2002). The columns are produced when the growth temperature is kept at about −6°C and plates are produced when the temperature is less than −10°C. The theoretical expectations shown in Fig. 1.4(b) and 1.4(c) are calculated with the ray-tracing method (Takano and Liou 1989) using particle habit statistics based on coincidently acquired images of the particles taken by a video microscope. The same 33-channel polar nephelometer used for the measurements of Fig. 1.4(a) was used for Figs. 1.4(b) and 1.4(c), but the 0.95 milliwatt unpolarized laser was replaced with a 35 milliwatt 670 nm unit with the polarization plane oriented parallel to the measurement plane. Both the theoretical and experimental results show the 22° intensity peak, which occurs from the refraction of light through the hexagonal faces that have a 60° angle between them, and the 46° peak which arises from re-

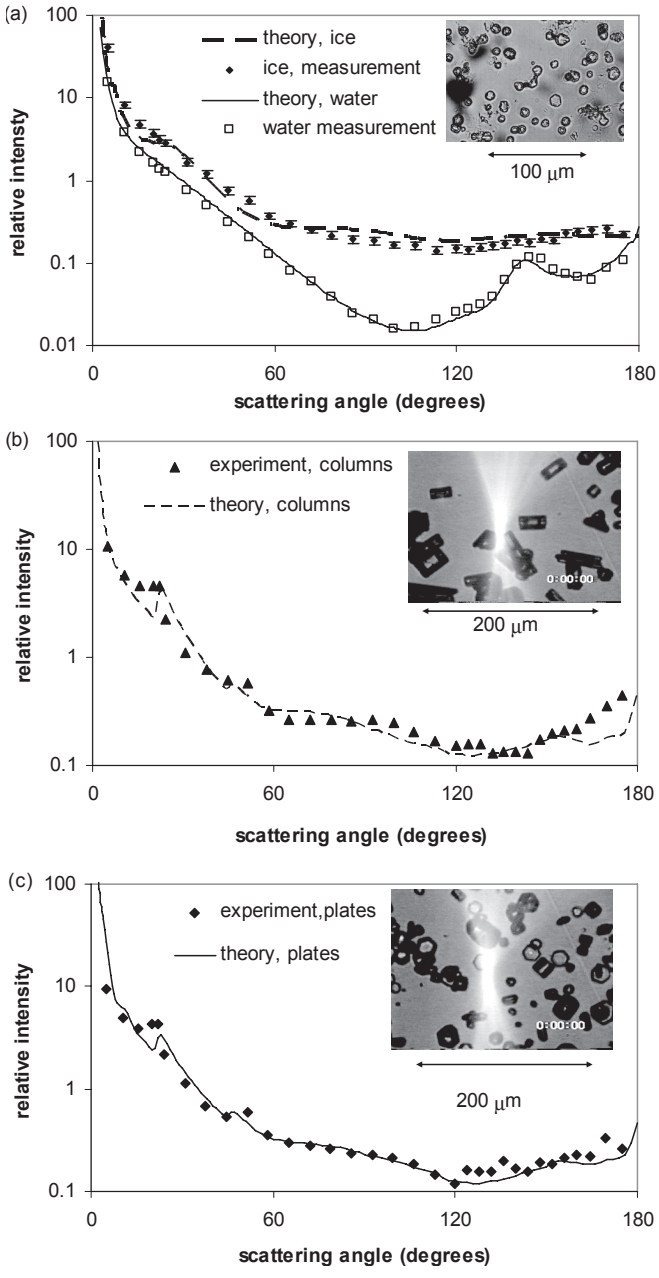

Fig. 1.4. (a) Measured and theoretical angular scattering properties of irregular ice crystals (♦) and water drops (♦) both with an average maximum dimension of about 7.5 μm. The incident 670 nm light is unpolarized and the theoretical expectations are fitted to the measurements using the method of least squares (Barkey and Liou 2001). (b) Measured and theoretical angular intensities with incident light polarized parallel to the measurement plane for ice particles that are predominately columnar in shape as seen in the image (Barkey et al. 2002). (c) is the same as (b) except for ice particles that are more plate like. Experimental and theoretical parameters are listed in Table 1.1.

fraction from end faces of the crystals that have a 90° angle between them. These refractions cause the halo or parhelia (or, more commonly, 'sun dogs') sometimes seen around the sun. Because the 60° faces occur more often than the 90° faces, the 22° intensity features in both Fig. 1.4(b) and 1.4(c) are more prominent than the 46° peak. The 46° peak for the column case (Fig. 1.4(c)) is less intense than that for the plate case because the occurrence of the 90° angle prisms are more prevalent for plates. Additionally, many of the columns have hollow ends as seen in the video image. Without these prisms, the intensity peaks are non-existent as seen for the irregular particle case seen in Fig. 1.4(a). The theoretical expectations, which are based on the observed particle habits, show similar relationships between the relative intensities of the halo features, thus providing direct verification of the complex ray-tracing algorithms on which they are based. Other polar nephelometer studies have also seen these halo intensity features in the laboratory (Sassen and Liou 1979a) and in the field (Gayet et al. 1998).

1.3.5.2 Aerosol scattering and inversion of PN data

Angular scattering information can be used to determine the optical and physical properties of particles. It has been shown theoretically that the determination of the real refractive index and size distribution parameters is possible from angular scattering measurements (Hodgson 2000; Shaw 1979) provided the particles are spherical and homogeneous. Spherical homogeneity allows the use of the Mie–Lorenz scattering solution. Researchers have successfully used several approaches to invert scattering data. These include direct inversion (Zhao 1999; Jones et al. 1994), manual trial and error (Kuik et al. 1991; Quinby-Hunt et al. 1997), table lookup (Verhaege et al. 2008) and optimization methods (Barkey et al. 2007; Lienert et al. 2003). The intensity of light as a function of the scattering angle is very sensitive to the size and composition of a single particle thus providing a means to study the particle's composition, optical properties and growth and evaporation rates (Pluchino 1987; Swanson et al. 1999).

An important application of PN measurements is the determination of the real refractive index of secondary organic aerosols (SOA). SOAs are ubiquitous in nature (Hallquist et al. 2009). While estimates of optical properties are available from organic materials with similarities to some of the components that make up complex SOA (Kanakidou et al. 2005) measurement of real SOA are few and until recently very rough. Shown in Fig. 1.5 are UCLA PN angular scattering measurements from SOA particles generated from ozonolysis of α-pinene in an outdoor solar reaction chamber. The particles grew from about 200 nm at 12:58 pm to about 450 nm in diameter at 14:55 pm. The experiment is discussed in detail in Kim et al. (2010). The retrieved real refractive index and fitness values for each plot are derived as described in section 1.4.2 below. The UCLA PN monitors scattering with incident light polarized both perpendicular (lower plot of each pair in Fig. 1.5) and parallel (upper plots) to the scattering plane. The earlier measurements are at the lower limit of the UCLA PN response. As the particle sizes and concentrations increase, the signal-to-noise ratio in the measurement increases and the angular scattering measurements become smoother. The 'shape' of the angular intensities change as the particles grow. For example the minimum intensity for the measured

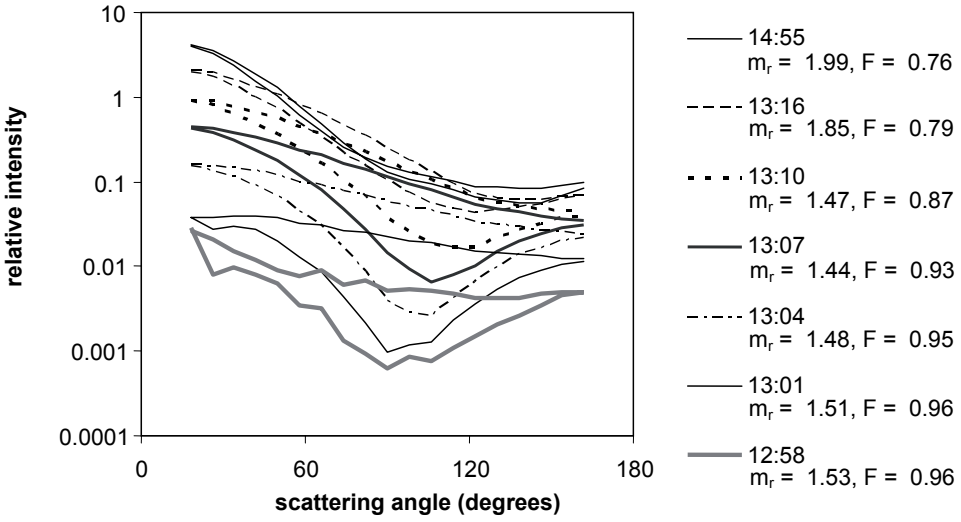

Fig. 1.5. UCLA PN scattering measurements of α-pinene-based SOA in which the particles grow from a diameter of about 200 nm at 12:58 pm to 450 nm at 14:55 pm. The two lines per time are with incident light polarized parallel (upper line) and perpendicular (lower line) to the measurement plane (Kim et al. 2010).

intensity with parallel incident light moves from about 90° to near 120° as the particle diameter increases. As the signal-to-noise ratio increases, the fitness value increases to near 0.96, indicating more confidence in the retrieved refractive index. A fitness value of '1' is optimal as described in section 1.4.2. This PN measurement is invaluable in not only providing values of the refractive indices for these volatile particles, but because of the fast response time of the measurement provides clues to the growth process of SOA.

1.4 UCLA polar nephelometer

This section describes the polar nephelometer (Fig. 1.6) developed at UCLA for the purpose of measuring the scattering properties of ice particles and aerosols. The first version was used had 33 fiber-optic light guides arranged to collect light scattered from 5° to 175° and was used to measure light scattering properties of ice particles as discussed above in section 1.3.5.1. Later, the instrument was modified to allow for the measurement of aerosol scattering. Enhancements included a sheath flow to better control the placement of the aerosols, installation of a higher power laser (670 nm, 350 milliwatts) and the incorporation of a half-wave plate and mechanical actuator to allow the incident light to be polarized parallel or perpendicular to the scattering plane. This prototype also replaced the fiber-optic light guides with detector aperture holes that more precisely controlled the angular resolution and greatly reduced the amount of stray light resulting from incomplete absorption of multiply reflected light in the scattering volume.

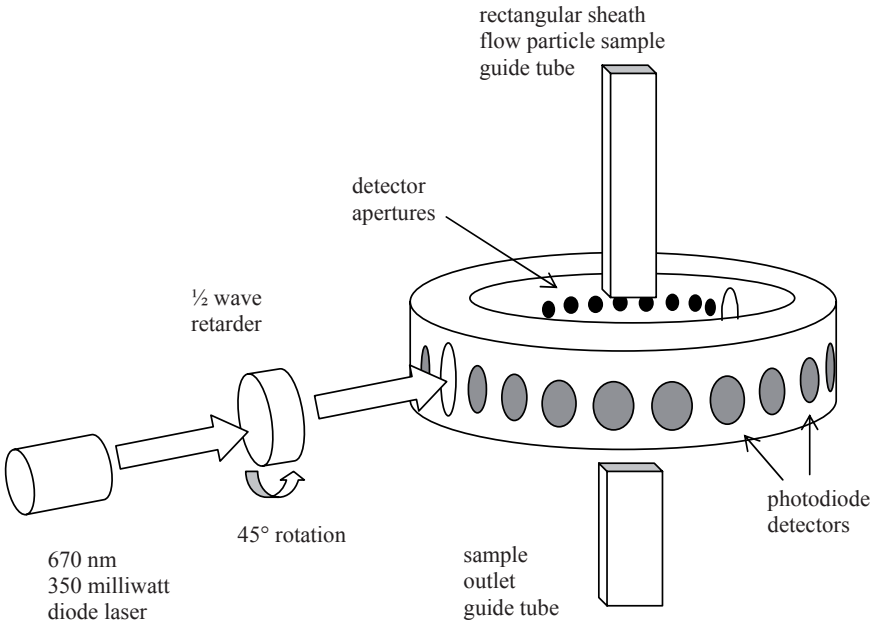

Fig. 1.6. Three-dimensional view of the UCLA polar nephelometer sensing geometry. The 21 photodetectors view the volume where the laser beam intersects the aerosol stream through 40 mm long holes that define the optical field of view. The aerosol stream is confined to the center of the detection array in a sheath flow. A half-wave plate rotates the polarization plane of the incident light to be either parallel or perpendicular to the detection plane.

1.4.1 Instrument description

The current UCLA polar nephelometer is an upgraded version of the unit described in (Barkey et al. 2007). Geometrically, the new polar nephelometer is similar to that unit but with significant improvements to the geometry, sample volume sealing and to the electromagnetic shielding to improve the sensitivity of the instrument. The original prototype was fabricated from plywood, while the new unit is machined to precise specifications from aluminum. The instrument consists of 21 large-area silicon photodiode detectors arranged in a two-dimensional plane (Figs. 1.6 and Fig. 1.2(b)) to measure the light scattered from a stream of particles that intersect a collimated laser beam directed across the plane. The stream of particles which is directed downwards perpendicular to the scattering plane is confined to the center of the array by a sheath flow of filtered air. The aerosol stream has a rectangular cross-section about 3 by 12 mm, oriented so that its long axis is parallel to the laser beam direction. The laser is easily changed. Data shown here was collected with a 350 milliwatt diode laser that directs a 670 nm wavelength beam of light with a profile height of about 3 mm and a width of 1 mm across the scattering volume. An electromechanically operated half-wave plate periodically changes the polarization plane of the incident light to be either parallel or perpendicular to the scattering measurement plane. The detectors are placed behind 40 mm long holes that act as apertures to define the field of view of each detector. The sensing

geometry is described above in section 1.2.1. Detector signals are amplified and an embedded computer and data acquisition system sends the measurements to an external PC for storage. The detectors are positioned to sense light scattered from 10° to 170° in 8° increments and have improved electromagnetic shielding such that the detector noise level is at least 10 times lower than the previous version. Single particle scattering as defined by Mishchenko et al. (2004) can be assumed because the detector distance to the sample volume (R_d) is about 75 mm, which is larger than the maximum dimension (12 mm) of the scattering volume. The average distance between each particle for a high particle concentration of $2.5 \times 10^6\,\mathrm{cm}^3$ is about 40 μm, which is much larger than the largest average particle size of about 0.5 μm. Finally $R_d/\lambda \gg 1$, where λ is the wavelength of the laser light.

1.4.2 Method of GA refractive index retrieval

The light scattered from a particle is dependent on the particle size, shape and refractive index. Real refractive indices (m_r) can be retrieved effectively using the genetic algorithm (GA) approach (Goldberg 1989). This optimization method has been shown to be effective despite the complex solution space of this problem and is effective in the presence of significant noise levels (Hodgson 2000). The GA method mimics the way in which biological systems find the 'best' individual. For instance, a 'population' of solutions consisting of real refractive indices and size distribution parameters are randomly selected from within a predefined search space. Then theoretical scattering expectations are determined for each 'member' and adjusted to match the UCLA PN sensing geometry as discussed in section 1.2.1. To date, we have primarily used the Mie–Lorenz method of determining the scattering properties for the spherical homogeneous particle, although any theoretical solution can be used as the GA method is an optimization scheme, and not a direct inversion. The particle size distribution for N particles with diameter d is assumed to be single mode lognormal via;

$$N(d,\mu,\sigma) = \frac{N}{x\sigma\sqrt{2\pi}}\,\exp\left[-\frac{1}{2}\left(\frac{\ln(d)-\mu}{\sigma}\right)^2\right] \tag{5}$$

in which $\mu = \sum_1^N N_i \ln(d_i)/N$ and, $\sigma = \left[\sum_1^N N_i(\mu - \ln(d_i))^2/N\right]^{1/2}$ are the mean and standard deviation of the log transformed size distribution data. Experimentally, size distribution data is usually obtained in discrete bins in which N_i is the number of particles in the bin centered about d_i. The parameters of each set are then compared to the measured scattering intensities with a fitness parameter defined via:

$$F_p = 1 - \frac{1}{N_c}\sum_{i=1}^{N_c} \left|\log\left(I_{p,thy}(\theta_i, m_r, \mu, \sigma)\right) - \log\left(I_{p,meas}(\theta_i)\right)\right| \tag{6}$$

for each scattering channel for $i = 1$ to N_c and the subscript 'p' indicates the polarization state of the incident light. $I_{p,thy}(\theta_i, m_r, \mu, \sigma)$ is the expected intensity value at the angular position θ_i as calculated via eq. (2) using the GA parameters m_r, μ and σ, and the Mie–Lorentz solution for scattering from a sphere. $I_{p,meas}(\theta_j)$

is fitted to the theory using the method of least squares. The log factor ensures that the fitness is not biased toward higher intensities (Lienert et al. 2003). The total fitness value is $F_t = (F_l + F_r)/2$, where r corresponds to the incident light polarized perpendicular to the scattering plane and l is for light polarized parallel. The population members with the best fitness values are digitally 'mated' to produce 'offspring' that should fit the solution better. The number of optimal members in the GA search population is determined operationally. For the case in which the sample is assured to be homogeneous and spherical and the size distribution is known, a population level of 40 to 50 is sufficient for the solution of synthetic results (discussed below) converging to the correct result in 3 generations. In practice, doubling the population level for experimental results assures convergence and successful retrieval has been demonstrated using both PSL particles and particles developed from a solution of ammonium sulfate and water. The GA results used in this paper are calculated using the C++ GA library developed by Wall (1996). Fig. 1.7 shows the measured scattering properties of ammonium sulfate water droplets ($(NH_4)_2SO_4$-H_2O). The droplets were generated from a mixture of 0.25% by weight ammonium sulfate in deionized water with a Colison (BGI Inc.) spray nebulizer and then partially dried by passage through a dessicant drier. Also shown are the GA determined angular scattering intensities determined using a population of 100 that ran for 3 generations. The retrieved $m_r = 1.414 \pm 0.03$, is in excellent agreement with the expected value of 1.414–1.413 for the measured relative humidity of about 60% (Tang and Munkelwitz 1991; 1994).

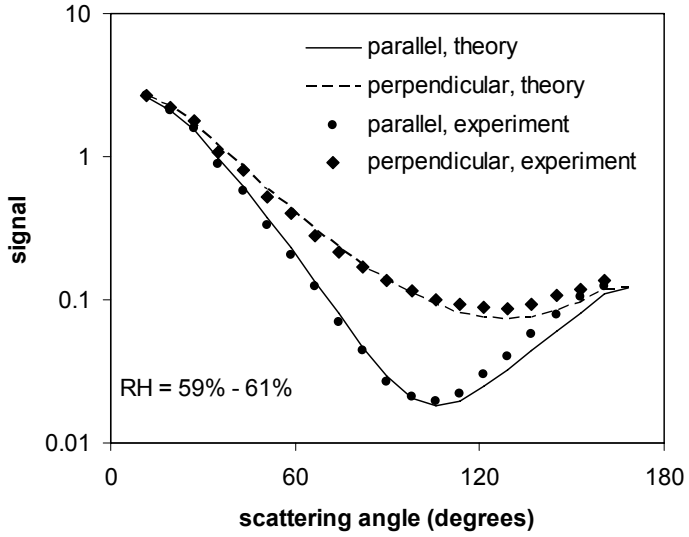

Fig. 1.7. The measured angular relative intensities from droplets consisting of a mixture of ammonium sulfate and water with the incident light polarized parallel (•) and perpendicular (⧫) to the measurement scattering plane. The lines indicate the expectation developed from a GA search of these experimental results in which a real refractive index of 1.414 ± 0.03 was found to fit the measurement. The expected value, based on the measured humidity, is 1.413 to 1.414 (Barkey et al. 2007).

1.4.3 Noise/accuracy analysis

Accuracy of the GA retrieved refractive index depends on errors from several sources including electronic noise, calibration errors, due to saturation in one or more of the detector channels or from the GA method itself. Measurements made at the lower limit of the instrument response have a low signal-to-noise ratio which for this instrument occurs when the signal voltage level is less than about 0.0001 Vdc. Also the zero light signal levels for each detector are not the same, which introduces an error that becomes more prominent at lower concentrations. At these low levels the measured intensities can be very different than the expectation despite extensive signal averaging. It has been shown that the GA retrieval of the real refractive index is insensitive to these low-intensity differences up to a maximum of 15% between the expected value and that measured (Barkey et al. 2007). Errors due to the GA retrieval method are also possible. The search space of a particular problem can be insufficiently searched, defined improperly, i.e., too wide or narrow, or the problem may be ill-constrained. Because the GA method is not an inversion scheme, it is possible for the problem to be ill-posed and for the GA program to still return an 'optimal' solution. The viability of the solution is checked by examining the convergence behavior of the GA retrieved values by performing the search several times and examining the %CV (100 $*$ standard deviation/average) of the retrieved values of any parameter of interest. If the solution is tenable, the GA search algorithm will converge to a single solution. For searches of theoretically derived data developed from the Mie–Lorentz scattering solution, the %CV of the m_r of 6 GA searches are less than 1%. These same theoretical GA results with noise synthetically applied can have %CV values from 2–5%. GA searches of scattering measurements of particles that are known to be spherical and homogeneous at the lower limit of the polar nephelometer sensitivity also have %CV values from 2–5%. Operationally it has been determined that %CV values greater than this means either the noise level is too high or the problem is ill-constrained.

Key to the accuracy analysis of the PN GA analysis scheme is the fact that the GA retrieval scheme is highly insensitive to instrument noise (Hodgson 2000). The retrieved result is based on the best fit of all of the data and is thus not unduly affected by erroneous data values. It has been shown that for this instrument the GA retrieval of m_r with detector noise levels of over 15% are accurate to within ± 0.03 (Barkey et al. 2007) as long as the particles are spherical and homogeneous. Thus, in the following analysis, as long as error levels are less than 15%, the m_r retrieval is accurate to within 0.03.

1.4.3.1 Errors due to calibration

Because the response of each detector is slightly different, deriving channel specific calibrations is necessary. Polystyrene latex (PSL) microspheres with well characterized size distributions and a manufacturer specified m_r of 1.5854 at 670 nm are used for this purpose. Shown in Fig. 1.8(a) is a plot of the light scattered by 800 nm in diameter PSL spheres (Duke Scientific Inc., 3800A) as measured by the PN before calibration and the Mie–Lorenz-determined scattering properties based on the manufacturer's specified size distribution parameters and refractive index. The

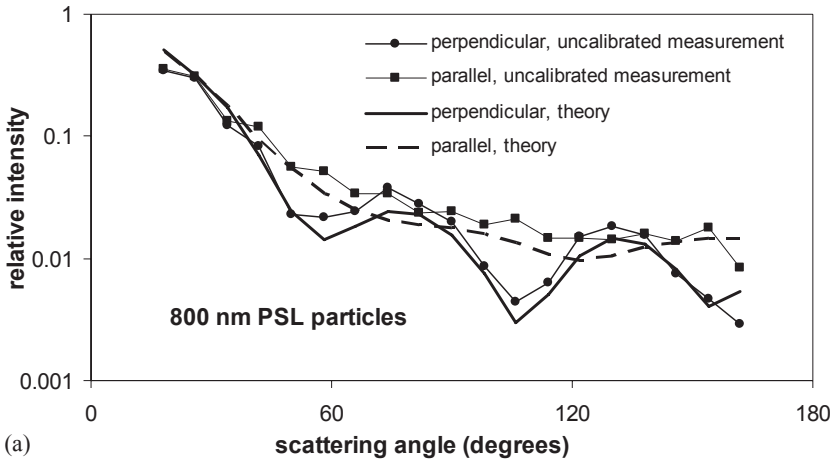

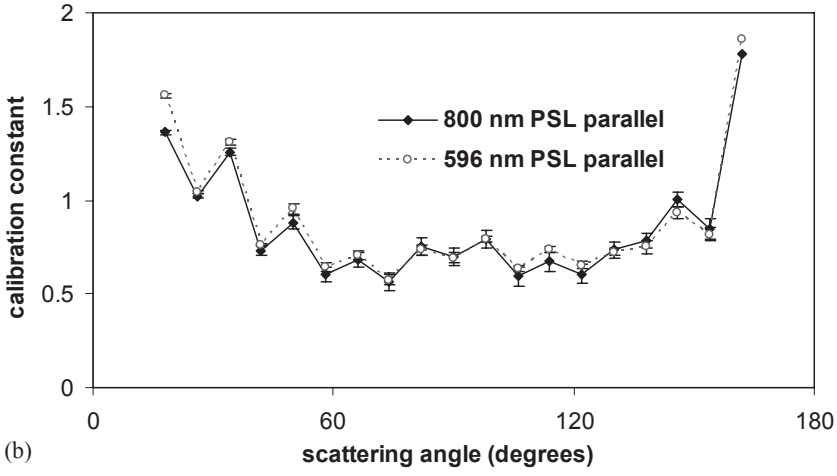

Fig. 1.8. (a) The measured uncalibrated angular scattering intensities from an almost monodisperse distribution of 800 nm in diameter PSL particles with the incident light polarized parallel and perpendicular to the scattering plane along with expectations using the Mie–Lorenz scattering solution based on the particle distribution and a refractive index of $1.5854 - i0.0$. (b) Multiplicative calibration constants developed separately from measurements of the 800 nm PSL particles and similar monodisperse PSL particles with a diameter of 596 nm. The calibration constants are similar showing that the detector response is not a function of the scattering particle size.

PSL particles were aerosolized in a Colison spray nebulizer (BGI Inc.) and then directed through sufficient desiccant tubes to dry them completely. Multiplicative calibration constants are developed from these measurements via:

$$C_i = \frac{I_{thy}(\theta_i, m_r, \mu, \sigma)}{I_{meas}(\theta_i)} \tag{7}$$

where μ and σ are from the manufacturers specifications, $I_{thy}(\theta_i,\ m_r,\ \mu,\ \sigma)$ are as defined in eq. (6) (as discussed in section 1.4.2) and $I_{meas}(\theta_i)$, is the intensity at detector i, which is linearly proportional to the measured voltage. The theoretical results are fitted to the measurement using the method of least squares. The values for the far forward (10°) and far reverse angles (170°) cannot be calibrated at this time due to their highly variable signals levels caused by laser beam drift. Work is under way to correct this problem. Shown in Fig. 1.8(b) are the calibration constants, ranging from about 0.5 to 1.8, developed using measurements of the 800 nm PSL particles (part a of Fig. 1.8), as well as for those developed using similar measurements of PSL particles with a mean diameter of 596 nm (Duke Scientific Inc., 5060A). These constants, C_i, correct the measured voltages to match voltages expected if each detector had identical response characteristics. These calibration constants should be similar to one another as the detector response should not be dependent on the particle size. Any differences in C_i are due to instrument noise or differences in the amount of unwanted signal from stray reflections within the scattering volume. Calibration constants are derived from scattering measurements that are relatively isotropic, i.e., the parallel incident light results of the 800 nm PSL particles shown in Fig. 1.8(a) rather than the highly variable scattering pattern for the perpendicular incident light for the same particle. Signal response at angles with low intensities (i.e., the dips near 60° and 100° in Fig. 1.8(a)) are more susceptible to noise and multiple internal reflections within the scattering volume and thus produce calibration constants that are very different from those derived from more isotropic scattering patterns. The average percent difference between the calibration constants for 596 nm and 800 nm PSL size particles is about 2.5%, with the maximum difference of 8% at 74°. These results indicate that spurious reflections within the scattering volume are at an acceptable level. Also, these error levels are well below 15% thus calibration errors do not contribute to m_r retrieval uncertainties greater than 0.03 as discussed above. PSL particles smaller than about 500 nm, are not used for calibration as they have a tendency to clump into 2 particle dimers which cannot be modeled with the single particle Mie–Lorenz solution.

1.4.3.2 The number of available channels

Although the laser power in the polar nephelometer can be adjusted over a range of about a factor of 10 and the instrument detectors have a dynamic range of about 5 decades, light scattered in the instrument can easily saturates the detectors in the forward and reverse directions. When this occurs, the saturated signal values are nonlinear and cannot be used in the refractive index retrieval. Therefore here we discuss a test of the number of channels required to accurately determine the real refractive index. The goal of this analysis is to determine the validity of the retrieved refractive index under the specific saturation conditions which are sometimes seen in our experiments.

Synthetic scattering intensities were developed using the Mie–Lorentz scattering theory for particles with a refractive index of $1.4 - i0.0$, and with a lognormal distribution average radius of 0.13 μm, and a standard deviation of 0.04 μm. These are similar to the particles seen in some of our aerosol experiments. Random noise

was applied to the synthetic scattering intensities using the following expression:

$$I'(\theta_i) = I(\theta_i)\,[1 + N_{\max}(1 - 2n_r)] \tag{8}$$

where $I(\theta_\iota)$ is the original non-noisy synthetic signal at scattering angle θ_i, $I(\theta_i)$ is the noisy result, $N_{\max}$ is the maximum noise level and n_r is a random number between 0 and 1. Fig. 1.9(a) shows the GA determined m_r vs. the number of missing channels. The channels are eliminated from the test in the manner in which they would saturate, i.e., the far forward channel at 10° is removed first, and then the far reverse channel at 170°, then the next forward channel and so on. As the retrieved value is within 0.015 of the expected m_r, it is seen that for synthetic data, the problem is over constrained and the fitness level during these test remain constant at about 0.99. A fitness value (F_t in eq. (9)) of 1.0 indicates a perfect fit. The high fitness value of 0.99 is expected for synthetic data that do not have calibration errors combined with the insensitivity of the GA method to noise as discussed above.

In Fig. 1.9(b) is a similar analysis of the number of available channels but using experimental data from aerosols formed from the ozonolysis of β-pinene without scavenger (Kim et al. 2010). The aerosols are generated in a 24 m^3 Teflon bag in which gaseous precursors are injected. When ozone was well mixed and its concentration became stable in the chamber, the hydrocarbon (β-pinene) was injected and the chamber mixed manually to minimize inhomogeneities. The GA retrieval of the refractive index for two PN measurements made once the particles had grown to 255 nm in diameter (labeled '255 nm' in Fig. 1.9(b)) at a particle concentration of about $9 \times 10^5\,\mathrm{cm}^{-3}$. Also shown is a similar result for particles formed earlier in the experiment when the particle mean diameter was about 145 nm at a lower concentration of $2 \times 10^5\,\mathrm{cm}^{-3}$. None of the detectors in any of these UCLA PN measurements were saturated. Because of the laser beam drift (above) the forward and reverse channels are not included hence the number of missing channels starts at 2 in Fig. 1.9(b). As in the synthetic case, the retrieved refractive index is relatively insensitive to the number of omitted channels although the retrieved m_r values varied about 0.042 for the 255 nm particles and 0.075 for the 145 nm particles. The range of the retrieved m_r for the synthetic results is 0.015. The retrieved m_r varies more with the number of missing channels for the 145 nm case than either the 255 nm cases or the synthetic cases which we believe is because there is more noise in the retrieved signal for the 145 nm case which had an overall smaller scattering signal. The fitness values for all the experimental cases range from 0.96 to 0.97.

1.4.4 GA retrieval of the imaginary index

In this section GA retrieval of synthetic data is used to determine how well the GA retrieval scheme can determine the real and imaginary (m_i) refractive indices of absorbing particles using data from the UCLA PN. There are many ways to measure the absorption (or imaginary component) of bulk materials (Toon et al, 1976) but aerosols do not come in the pure state of the measured components and are often mixed inhomogeneously with various, often unknown materials. Therefore there is a need for measuring the absorption component of materials in their aerosol state.

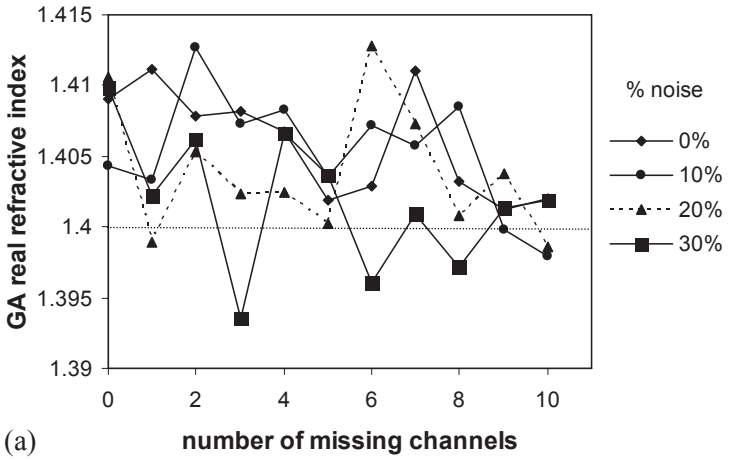

(a)

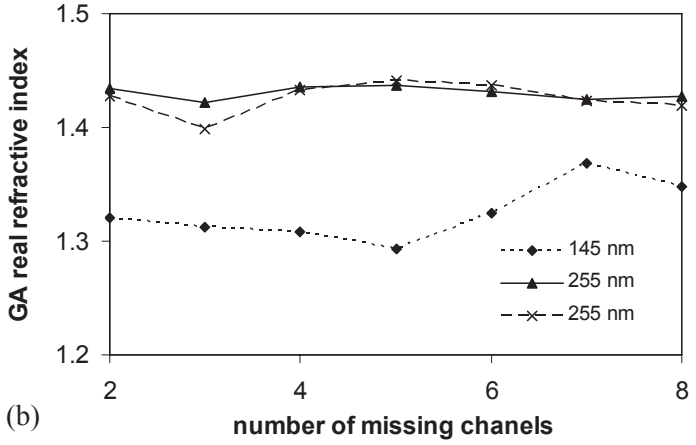

(b)

Fig. 1.9. (a) The GA determined real refractive index for Mie–Lorenz synthetic results developed for particles with a refractive index of $1.4 - i0.0$. It is seen that the inversion problem is overdetermined as the GA retrieved m_r are within 0.015 of the expected value even when the number of missing channels or data points is increased to 10. (b) The same as (a) but for experimental measurements of α-pinene based secondary organic aerosol at 3 points in its growth cycle where the measured particle mean diameter is indicated.

Cavity ring down technology offers the capability to measure the extinction properties of ambient level aerosols in reasonable path lengths and are well suited for this task (Abo Riziq et al. 2007; Lang-Yona 2010). A previous attempt at retrieval of the imaginary component by (Jones et al. 1994) was unsuccessful, but the instrument in that study had only one incident polarization. (Zhao 1999) however achieved success by the including several Stokes parameters in his measurement; however, the accuracy of the imaginary component was only 50%. A sensitivity analysis of the retrieval capabilities of the imaginary index using another goniometer type dual

polarization nephelometer design was shown to be possible for particles with moderate absorption, $10^{-4} \leq m_i \leq 0.5$ (Verhaege et al. 2008). Thus, the possibility of determining the imaginary component of the refractive index is dependent on the instrument configuration and which scattering properties are measured. In order to determine the feasibility of m_i determination with the UCLA PN, a sensitivity test is performed on synthetic data. Finally the refractive index developed from the GA inversion of aerosolized nigrosin is presented.

1.4.4.1 Theoretical examination of the search space

Synthetic data for aerosol particles with a refractive index of 1.7−i0.3 was generated for lognormal size distributions with mean and standard deviation values between 20 and 140 nm in 10 nm steps. The size distribution parameters are based on the sizes common to our experiments. The refractive index was chosen to be similar to that of nigrosin, which is a short-chain polyaniline compound consisting of 8 nitrogen-linked aromatic carbon rings ($C_{48}N_9H_{51}$) (Bond et al. 1999). Nigrosin forms spheres when aerosolized by the Colison nebulizer and dried completely when passed through a dessicant drier. The measured refractive index varies from 1.65 to 1.7 in the real part and from 0.24 to 0.31 in the imaginary component (Abo Riziq et al. 2007; Garvey and Pinnick 1983; Lack et al. 2006). The GA search was performed with a population of 50 and ran for 3 generations. A noise level of 15% is applied to the synthetic data as described by eq. (8). Shown in Fig. 1.10(a) is a plot of the retrieved average m_i of 6 separate GA searches of these synthetic data at each distribution size and standard deviation. The results show that the imaginary component is returned reasonably accurately for most combinations of the mean and standard deviation (within 7% for standard deviations greater than 50 nm), however for narrow distributions, the retrieval becomes consistently inaccurate and can deviate from the expected value by over 200%.

In Fig. 1.10(b) is shown the %CV of the 6 searches, indicating the convergence properties of the GA retrieval as discussed above in section 1.4.3. As in the m_i retrieval, the uncertainty increases as the distribution width narrows. For standard deviations values greater than 50 nm, the average %CV is about 15%, however, the maximum %CV is over 50% at the larger mean sizes in this region. The real refractive index (not shown) is much better retrieved with an average $m_r = 1.70 \pm 0.02$ when the standard deviation is greater than 60 nm. The %CV for the m_r retrievals is about 2.5%. As in the imaginary case, the GA m_r retrievals are slightly more uncertain for smaller standard deviations.

These results are somewhat contrary to the results of Verhaege et al. (2008) who have shown that the retrieval of the real and imaginary component of the refractive index is possible with moderate absorption ($10^{-4} \leq m_i \leq 0.5$) while our results show that the retrieved imaginary component is uncertain by at least 10%, but often by much more. There are several possible reasons for this, our retrieval method and experimental setup is different and we have not analyzed a large space of possible mean sizes, refractive indices and distributions widths, only those that we have seen in our experiments. Also, the resolution of this experimental study (i.e., the 10-nm step size in the mean and standard deviation) is much larger than that in the Verhaege study. There may be a localized minimum in the %CV of GA retrieval that we have missed.

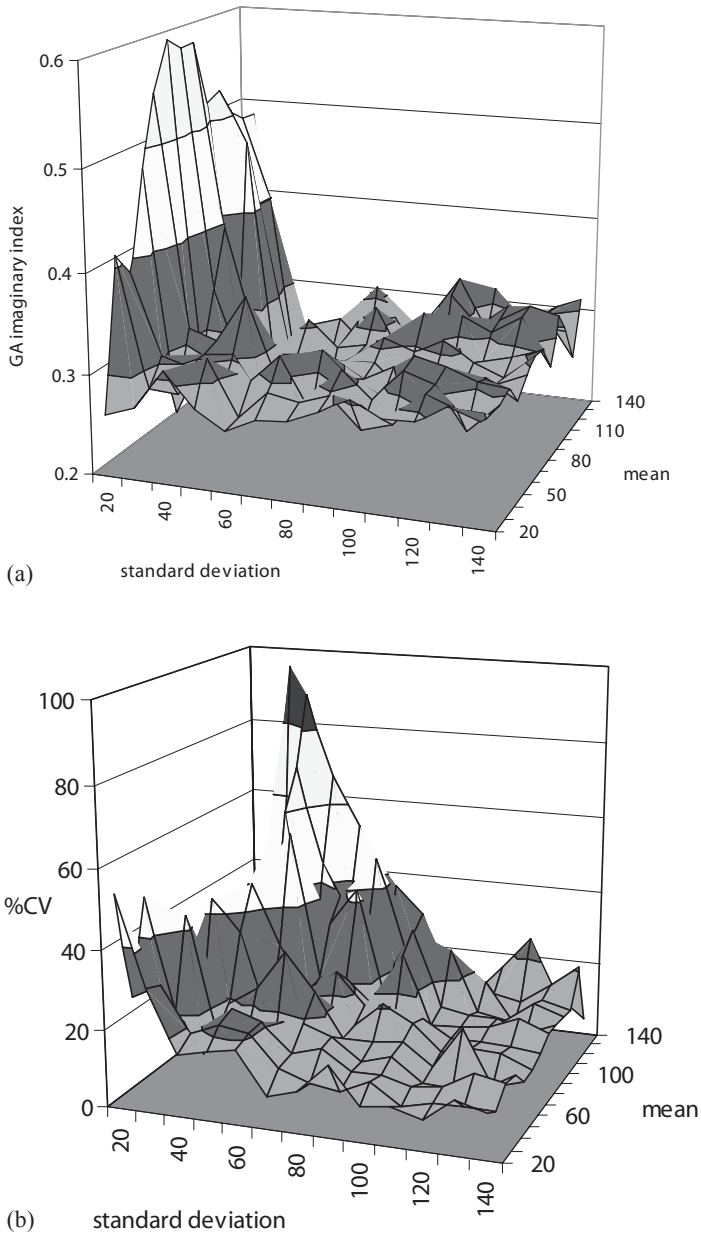

Fig. 1.10. (a) The GA determined imaginary refractive index for Mie–Lorenz-based synthetic results for particles with a refractive index similar to that of nigrosin ($1.7 - i0.3$) for distribution parameters chosen to be similar to those seen in our experiments. Except for the distributions with standard deviations less than 60 nm, the maximum retrieved m_i is 0.33 and the minimum is 0.23. (b) The %CV of 6 separate searches for the m_i in part (a). As in part (a), the %CV, or uncertainty in the retrieved m_i due to the inversion being ill-posed is much higher for the narrower distributions.

1.4.4.2 Experimental results

Droplets of nigrosin and water from a Colison spray aerosolizer are sent through a dessicant drier and then separately sized by a scanning mobility particle sizer (SMPS, TSI Inc. Model 3080) or sent to the UCLA PN. Various particle distribution mean sizes and widths were generated by varying the concentration of the nigrosin in the solution. GA searches for the real and imaginary refractive indices using a population of 200 for 3 generations was performed for the measured PN angular scattering data. The size distribution search space was set at ±5% of the SMPS mean size and standard deviation as listed in Table 1.5. As expected, in Table 1.5, the real refractive indices were determined more accurately than the imaginary component. In almost all cases the levels of error are much higher than the errors seen in the theoretical study. This may arise from a handful of sources, the synthetic results do not have any noise or effects from multiple internal reflections, the actual refractive index of the nigrosin may be somewhat different from the accepted value due to batch-to-batch variations in the nigrosin, and the fact that it is difficult to be certain the particles are completely dry, and the particle size distributions may be distorted from lognormal. The retrieved refractive index values for the particles with the largest sizes differ more than the smaller sizes from the expected value, and their fitness values are lowest in these tests, which is probably because at these larger sizes, the measured distributions exhibit a dual mode behavior. A study of how distortions in the distribution, i.e., departure from lognormal, have been done for non-absorbing particles (Barkey et al. 2010). It was shown that widening the GA search space on both the measured mean and standard deviation beyond the SMPS accepted error of ±5% for UCLA PN measurements made from aerosols with distorted distributions (within a quantifiable level) can be done to retrieve the real refractive index to within 0.014. However, this analysis has yet to be performed for absorbing particles.

Table 1.5. GA determined nigrosin real and imagined refractive indicies from experimental measurements.

Mean diameter (nm)	Standard deviation	GA m_r	%difference*	GA m_i	%difference**	Fitness
71.0	38.5	1.54	8%	0.45	73%	0.94
47.7	21.9	1.56	7%	0.40	54%	0.96
70.7	38.1	1.63	3%	0.48	86%	0.92
72.9	39.4	1.59	5%	0.52	100%	0.92
134.0	96.0	1.69	1%	0.46	75%	0.96
136.8	126.2	1.43	14%	0.07	74%	0.88
112.0	94.0	1.40	16%	0.15	41%	0.83

* Percent difference between GA determined m_r and the accepted value of 1.67.
** Percent difference between the GA determined m_i and the accepted value of 0.26.

1.4.4.3 Discussion of the retrieval of the imaginary index

The UCLA PN and the GA retrieval method of determining the real refractive index has been shown to be accurate to within ± 0.03 for particles which are known to be spherical and homogeneous. Uncertainties arising from errors in the calibration, from instrument noise and from missing, i.e., saturated, channels affect the retrieved refractive indices only slightly because of the insensitivity of the GA retrieval method to noise and because this retrieval problem is over-constrained. Preliminary studies of the effectiveness of the retrieval of the imaginary component of the refractive index is at most accurate to within 10% under optimal, i.e., no noise, conditions. Experimentally, however, errors up to 100% in the retrieved value of the index are seen although additional investigations may yield more accurate retrievals in the future. Within the size limits seen, in our laboratory, the retrieval accuracy of the imaginary refractive index is more dependent on the mean size and standard deviation of the measured particles than is the real part.

Acknowledgments

We would like to thank Hwajin Kim for her extensive help with the secondary organic aerosol experiments. This review included many projects funded by various agencies: US Department of Energy's Atmospheric Science Program (Office of Science, BER, Grant No. DE-FG02-05ER64011); National Science Foundation grant ATM-9907924; US Air Force Office of Scientific Research grant F499620-98-1-0232.

References

Abo Riziq, A., C. Erlick, E. Dinar, and Y. Rudich, 2007: Optical properties of absorbing and non-absorbing aerosols retrieved by cavity ring down (CRD) spectroscopy. *Atmos. Chem. Phys.*, **7**, 1523–1536.

Aden, A. L., and M. Kerker, 1951: Scattering of electromagnetic waves from two concentric spheres. *J. Appl. Phys.*, **22**, 1242–1246.

Bacon, N. J., and B. D. Swanson, 2000: Laboratory measurements of light scattering by single levitated ice crystals, *J. Atmos. Sci.*, **57**, 2094–2104.

Bacon, N. J., B. D. Swanson, M. B. Baker, and E. J. Davis. 1998: Laboratory measurements of light scattering by single ice particles. *J. Aerosol Sci., Proceedings of the 1998 International Aerosol Conference Part 2,* 29, S1317-S1318.

Baran, A. J., P. Yang, and S. Havemann, 2001: Calculation of the single-scattering properties of randomly oriented hexagonal ice columns: A comparison of the T-matrix and the finite-difference time-domain methods. *Appl. Opt.*, **40**, 4376–4386. doi:10.1364/AO.40.004376.

Barkey, B., H. Kim, and S. E. Paulson, 2010: Genetic algorithm retrieval of real refractive Index from aerosol distributions that are not lognormal. *Aerosol Sci. Technol.*, **44**, 1089–1095.

Barkey, B., S. E. Paulson, and A. Chung, 2007: Genetic algorithm inversion of dual polarization polar nephelometer data to determine aerosol refractive index. *Aerosol Sci. Technol.*, **41**, 751–760.

Barkey, B., M. Bailey, K. N. Liou, and J. Hallett, 2002: Light scattering properties of plate and column ice crystals generated in a laboratory cold chamber. *Appl. Opt.*, **41**, 5792–5796.

Barkey, B., and K. N. Liou, 2001: Polar nephelometer for light-scattering measurements of ice crystals. *Opt. Lett.*, **26**, 232–234.

Barkey, B., K. N. Liou, W. Gellerman, and P. Sokolsky, 1999: An analog light scattering experiment of hexagonal icelike particles. Part I: Experimental apparatus and test measurements. *J. Atmos. Sci.*, **56**, 605–612.

Bond, T. C., T. L. Anderson and D. Campbell, 1999: Calibration and intercomparison of filter-based measurements of visible light absorption by aerosols. *Aerosol Sci. Technol.*, **30**, 582–600.

Bond, T. C., G. Habib, and R. W. Bergstrom, 2006: Limitations in the enhancement of visible light absorption due to mixing state. *J. Geophys. Res.*, **111**, D20211. doi:10.1029/2006JD007315.

Borghesi, A., and G. Guizzetti, 1991: *Graphite in Handbook of Optical Constants of Solids II.* San Diego: Academic Press.

Bukatyi, V. I., Y. D. Kopytin and V. A Pogodaev, 1983: Combustion of carbon particles initiated by laser radiation. *Russ. Phy. J.*, **26**, 113–120.

Castagner, J. and I. J Bigio, 2006: Polar nephelometer based on a rotational confocal imaging setup. *Appl. Opt.*, **45**, 2232–2239.

Castagner, J. and I. J Bigio, 2007: Particle sizing with a fast polar nephelometer. *Appl. Opt.*, **46**, 527–532.

Chae, S., and H. S. Lee, 1993: Determination of refractive indices of dyed polymer onospheres. *Aerosol Sci. Technol.* **18**, 403–417. doi:10.1080/02786829308959613.

Chỳlek, P., V. Srivastava, R. G. Pinnick, and R. T. Wang, 1988: Scattering of electromagnetic waves by composite spherical particles: experiment and effective medium approximations. *Appl. Opt.*, **27**, 2396–2404.

Colak, S., C. Yeh, and L. W. Casperson, 1979: Scattering of focused beams by tenuous particles. *Appl. Opt.* **18**, 294–302. doi:10.1364/AO.18.000294.

Curtis, D. B., M. Aycibin, M. A. Young, V. H. Grassian, and P. D. Kleiber, 2007: Simultaneous measurement of light-scattering properties and particle size distribution for aerosols: Application to ammonium sulfate and quartz aerosol particles. *Atmos. Environ.* **41**, 4748–4758.

Dick, W. D., P. J. Ziemann, and P. H. McMurry, 1998: Shape and refractive index of submicron atmospheric aerosols from multiangle light scattering measurements. *J. Aerosol Sci.*, **29**, S103–S104. doi:10.1016/S0021-8502(98)00148-7.

Dick, W. D., P. J. Ziemann, and P. H. McMurry, 2007: Multiangle light-scattering measurements of refractive index of submicron atmospheric particles. *Aerosol Sci. Technol.*, **41**, 549. doi:10.1080/02786820701272012.

Dugin, V. P., B. M. Golubitskiy, S. O. Mirumyants, P. I. Paramonov and M. V. Tantashev, 1971: Optical properties of artificial ice clouds, *Bull. (Izv.) Acad. Sci. USSR, Atmospheric and Oceanic Physics,* **7**, 871–877.

Dugin, V. P., and S. O. Mirumyants, 1976: The light scattering matrices of artificial crystalline clouds. *Bull. (Izv.) Acad. Sci. USSR, Atmospheric and Oceanic Physics*, **9**, 988–991.

Dugin, V. P., O. A. Volkovitskiy, S. O. Mirumyants and N. K. Nikiforova, 1977: Anisotropy of light scattering by artificial crystalline clouds. *Bull. (Izv.) Acad. Sci. USSR, Atmospheric and Oceanic Physics*, **13**, 22–25.

Fuller, K. A., W. C. Malm and S. M. Kreidenweiss, 1999: Effects of mixing on extinction by carbonaceous particles. *J. Geophys. Res.*, **104**, 15941–15954.

Garrett, T. J., H. Gerber, D. G. Baumgardner, C. H. Twohy and E. M. Weinstock, 2003: Small, highly reflective ice crystals in low-latitude cirrus, *Geophys. Res. Lett.*, **30**, 2132, doi:10.1029/2003GL018153.

Garvey, D. M., and R. G. Pinnick, 1983: Response characteristics of the particle measuring systems active scattering aerosol spectrometer probe (ASASP–X). *Aerosol Sci. Technol.*, **2**, 477. doi:10.1080/02786828308958651.

Gayet, J.-F., F. Auriol, S. Oshchepkov, F. Schröder, C. Duroure, G. Febvre, J.-F. Fournol, O. Crėpel, P. Personne, and D. Daugereon, 1998: In situ measurements of the scattering phase function of stratocumulus, contrails and cirrus. *Geophys. Res. Lett.*, **25**, 971–974.

Goldberg, D. E., 1989: *Genetic Algorithms in Search, Optimization, and Machine Learning*, 1st edn. Reading, MA: Addison-Wesley.

Gorchakov, G. I., 1966: Light scattering matrices in the atmospheric surface layer. *Bull. (Izv.) Acad. Sci. USSR, Atmospheric and Oceanic Physics,* **2**, 595–605.

Hallquist, M., J. C. Wenger, U. Baltensperger, Y. Rudich, D. Simpson, M. Claeys, J. Dommen, et al., 2009: The formation, properties and impact of secondary organic aerosol: current and emerging issues. *Atmos. Chem. Phys.*, **9**, 5155–5236.

Hansen, J. E. and A. A. Lacis, 1990: Sun and dust versus greenhouse gases: an assessment of their relative roles in global climate change. *Nature,* **346**, 713–719. doi:10.1038/346713a0.

Hansen, M. Z. and W. H. Evans, 1980: Polar nephelometer for atmospheric particulate studies. *Appl. Opt.*, **19**, 3389–3395. doi:10.1364/AO.19.003389.

Hirst, E., P. H Kaye and J. R Guppy, 1994: Light scattering from nonspherical airborne particles: Experimental and theoretical comparisons. *Appl. Opt.*, **33**, 7180.

Hodgson, R. J. W., 2000: Genetic algorithm approach to particle identification by light scattering, *J. Colloid Interface Sci.*, **229**, 399–406.

Holland, A. C., and G. Gagne, 1970: The scattering of polarized light by polydisperse systems of irregular particles. *Appl. Opt.* **9**, 1113–1121. doi:10.1364/AO.9.001113.

Holland, A. C., and J. S. Draper, 1967: Analytical and experimental investigation of light scattering from polydispersions of mie particles. *Appl. Opt.* **6**, 511–518. doi:10.1364/AO.6.000511.

Horvath, H., 1993: Atmospheric light absorption-A review. *Atmos. Environ.*, **27a**, 293–317.

Hovenier, J. W., H. Volten, O. MuÚoz, W. J. van der Zande, and L. B. Waters, 2003: Laboratory studies of scattering matrices for randomly oriented particles: Potentials, problems, and perspectives. *J. Quant. Spectrosc. Radiat. Transfer*, **79–80**. Electromagnetic and Light Scattering by Non-Spherical Particles, 741–755.

Huffman, P., 1970: Polarization of light scattered by ice crystals. *J. Atmos. Sci.*, **27**, 1207–1208.

Hunt, A. J. and D. R. Huffman, 1973. A new polarization-modulated light scattering instrument. *Rev. Sci. Instrum.*, **44**, 1753–1762.

Jones, M. R., K. H. Leong, M. Q. Brewster and B. P. Curry, 1994: Inversion of light-scattering measurements for particle size and optical constants: Experimental study. *Appl. Opt.*, **33**, 4035–4041.

Kaller, W., 2004: A new polar nephelometer for measurement of atmospheric aerosols. *J. Quant. Spectrosc. Radiat. Transfer,* **87**, 107–117.

Kanakidou, M., J. H. Seinfeld, S. N. Pandis, I. Barnes, F. J. Dentener, M. C. Facchini, R. Van Dingenen, et al., 2005: Organic aerosol and global climate modelling: A review. *Atmos. Chem. Phys.* **5**, 1053–1123.

Kaye, P. H., E. Hirst, J. M. Clark, and F. Micheli, 1992: Airborne particle shape and size classification from spatial light scattering profiles. *J. Aerosol Sci.*, **23**, 597–611.

Kim, H., B. Barkey, and S. E. Paulson, 2010. Real refractive indices of α- and β-pinene and toluene secondary organic aerosols generated from ozonolysis and photo-oxidation (in press).

Klett, J. D., 1995: Orientation model for particles in turbulence. *J. Atmos. Sci.*, **52**, 2276–2285.

Kuik, F., P. Stammes and J. W Hovenier, 1991: Experimental determination of scattering matrices of water droplets and quartz particles. *Appl. Opt.*, **30**, 4872–4881.

Lack, D. A., E. R. Lovejoy, T. Baynard, A. Pettersson and A. R. Ravishankara, 2006: Aerosol absorption measurement using photoacoustic spectroscopy: Sensitivity, calibration and uncertainty developments. *Aerosol Sci. Technol.*, **40**, 697. doi:10.1080/02786820600803917.

Lack, D. A., C. D. Cappa, D. Christopher, E. B. Cross, P. Massoli, A. T. Ahern, P. Davidovits and T. B. Onasch, 2009: Absorption enhancement of coated absorbing aerosols: Validation of the photo-acoustic technique for measuring the enhancement, *Aerosol Sci. Technol.*, **43**, 1006–1012.

Lang-Yona, N., Y. Rudich, Th. F. Mentel, A., Bohne, A. Buchholz, A. Kiendler-Scharr, E. Kleist, C. Spindler, R. Tillmann, and J. Wildt, 2010: The chemical and microphysical properties of secondary organic aerosols from Holm Oak emissions, *Atmos. Chem. Phys.*, **10**, 7253–7265, doi:10.5194/acp-10-7253-2010.

Leong, K. H., M. R. Jones, D. J. Holdridge and M. Ivey, 1995: Design and test of a polar nephelometer. *Aerosol Sci. Technol.*, **23**, 341–356.

Lienert, B. R, J. N Porter and S. K Sharma, 2003: Aerosol size distributions from genetic inversion of polar nephelometer data. *J. Atmos. Oceanic Technol.*, **20**, 1403–1410.

Liou, K. N., 1975: Theory of the scattering-phase-matrix determination for ice crystals. *J. Opt. Soc. Am.*, **65**, 159–162.

Liou, K. N., 1986: Influence of cirrus clouds on weather and climate processes: A global perspective. *Mon. Weather Rev.*, **114**, 1167–1199.

Liou, K. N., Y. Takano and P. Yang, 1999: Light scattering and radiative transfer in ice crystal clouds: Applications to climate research. In *Light Scattering by Nonspherical Particles: Theory, Measurements and Applications*, ed. M. I. Mishchenko, J. W. Hovenier and L. D. Travis, 417–449. New York: Academic Press.

Liu, L. and M. Mishchenko, 2005: Effects of aggregation on scattering and radiative properties of soot aerosols. *J. Geophys. Res.*, **110**, D11211. doi:10.1029/2004JD005649.

Lushnikov, A.A. and A.E. Negin, 1993: Aerosols in strong laser beams. *J. Aerosol Sci.*, **24**, 707–735. doi: 10.1016/0021-8502(93)90042-8.

Marshall, S. F., D. S. Covert and R. J. Charlson, 1995: Relationship between asymmetry parameter and hemispheric backscatter ratio: implications for climate forcing by aerosols. *Appl. Opt.*, **34**, 6306–6311. doi:10.1364/AO.34.006306.

Mie, Gustav, 1908. Beiträge zur optik trüber medien, speziell kolloidaler metallösungen. *Annalen der Physik*, **330**, 377–445.

Mishchenko, M. I., 1991: Light scattering by randomly oriented axially symmetric particles. *J. Opt. Soc. Am. A,* **8**, 871–882. doi:10.1364/JOSAA.8.000871.

Mishchenko, M. I., A. A. Lacis, B. E. Carlson and L. D. Travis, 1995: Nonsphericity of dust-like tropospheric aerosols: Implications for aerosol remote sensing and climate modeling. *Geophys. Res. Lett.*, **22**, 1077-1080.

Mishchenko, M. I., J. W. Hovenier and D. W. Mackowski, 2004: Single scattering by a small volume element. *J. Opt. Soc. Am. A,* **21**, 71–87. doi:10.1364/JOSAA.21.000071.

Nakaya, U., 1954. *Snow Crystals*. Harvard Univerity Press.

Ou, S. C., K. N. Liou, Y. Takano and R. L. Slonaker, 2005: Remote sensing of cirrus cloud particle size and optical depth using polarimetric sensor measurements. *J. Atmos. Sci.*, **62**, 4371–4383.

Perrin, F., 1942: Polarization of light scattered by isotropic opalescent media. *J. Chem. Phys.*, **10**, 415. doi:10.1063/1.1723743.

Perry, R. J., A. J. Hunt and D. R. Huffman, 1978. Experimental determinations of Mueller scattering matrices for nonspherical particles. *Appl. Opt.*, **17**, 2700–2710.

Pluchino, A. B., 1987. Scattering photometer for measuring single ice crystals and evaporation and condensation rates of liquid droplets. *J. Opt. Soc. Am. A,* **4**, 614.

Quinby-Hunt, M. S., L. L. Erskine and A. J. Hunt, 1997. Polarized light scattering by aerosols in the marine atmospheric boundary layer. *Appl. Opt.*, **36**, 5168–5184.

Sassen, K. and K. N. Liou, 1979a. Scattering of polarized laser light by water droplet, mixed-phase and ice crystal clouds. Part I: Angular scattering patterns. *J. Atmos. Sci.*, **36**, 838–851.

Sassen, K. and K. N. Liou, 1979b. Scattering of polarized laser light by water droplet, mixed-phase and ice crystal clouds. Part II: Angular depolarizing and multiple-scattering behavior. *J. Atmos. Sci.*, **36**, 852–861.

Schnaiter, M. and G. Wurm, 2002: Experiments on light scattering and extinction by small, micrometer-sized aggregates of spheres. *Appl. Opt.* **41**, 1175–1180.

Seinfeld, J. H. and S. N. Pandis, 1998: *Atmospheric Chemistry and Physics: From Air Pollution to Climate Change.* New York: John Wiley.

Shaw, G. E., 1979. Inversion of optical scattering and spectral extinction measurements to recover aerosol size spectra. *Appl. Opt.*, **18**, 988–993. doi:10.1364/AO.18.000988.

Spindler, C., A. Abo Riziq and Y. Rudich, 2007: Retrieval of aerosol complex refractive index by combining cavity ring down aerosol spectrometer measurements with full size distribution information. *Aerosol Sci. Technol.* **41**, 1011–1017.

Swanson, B. D., N. J. Bacon, E. J. Davis and M. B. Baker, 1999: Electrodynamic trapping and manipulation of ice crystals. *Q. J. R. Meteorolog. Soc.*, **125**, 1039–1058.

Szymanski, W. W., A. Nagy, A. Czitrovszky and P. Pani, 2002: A new method for the simultaneous measurement of aerosol particle size, complex refractive index and particle density. *Meas. Sci. Technol.* **13**, 303–307.

Takahashi, T., and N. Fukuta, 1988: Ice crystal replication with common plastic solutions. *J. Atmos. Oceanic Technol.*, **5**, 129–135.

Takano, Y., and K. N. Liou, 1989: Solar radiative transfer in cirrus clouds. Part I: Single-scattering and optical properties of hexagonal ice crystals. *J. Atmos. Sci.*, **46**, 3–19.

Tanaka, M., T. Takamura and T. Nakajima, 1983: Refractive index and size distribution of aerosols as estimated from light scattering measurements. *J. Climate Appl. Meteor.*, **22**, 1253–1261.

Tang, I. N., and H. R. Munkelwitz, 1991: Simultaneous determination of refractive index and density of an evaporating aqueous solution droplet. *Aerosol Sci. Technol.*, **15**, 201. doi:10.1080/02786829108959527.

Tang, I. N. and H. R. Munkelwitz, 1994: Water activities, densities, and refractive indices of aqueous sulfates and sodium nitrate droplets of atmospheric importance. *J. Geophys. Res.*, **99**, 18801–18808.

Toon, O., J. Pollack and B Khare. 1976: The optical constants of several atmospheric aerosol species: Ammonium sulfate, aluminum oxide, and sodium chloride. *J. Geophys. Res.*, **81**, 5733–5748.

Van de Hulst, H. C., 1957: *Light Scattering by Small Particles.* New York: John Wiley.

Verhaege, C., V. Shcherbakov and P. Personne, 2008: Limitations on retrieval of complex refractive index of spherical particles from scattering measurements. *J. Quant. Spectrosc. Radiat. Transfer,* **109**, 2338–2348. doi:10.1016/j.jqsrt.2008.05.009.

Volten, H., O. MuÚoz, E. Rol, J. F. de Haan, W. Vassen, J. W. Hovenier, K. Muinonen and T. Nousiainen, 2001: Scattering matrices of mineral aerosol particles at 441.6 nm and 632.8 nm. *J. Geophys. Res.*, **106**, 17,375–17,401.

Wall, M., 1996: *Galib: A C++ Library of Genetic Algorithm Components,* Mechanical Engineering Department, Massachusetts Institute of Technology. http://lancet.mit.edu/galib-2.4/

Warren, S. G., and R. E. Brandt, 2008: Optical constants of ice from the ultraviolet to the microwave: A revised compilation. *J. Geophys. Res.*, **113**, D14220, doi:10.1029/2007JD009744.

West, R. L, L. Doose, A. Eibl, M. Tomasko and M. Mishchenko, 1997: Laboratory measurements of mineral dust scattering phase function and linear polarization. *J. Geophys. Res.*, **102**, 16871–16881.

Yang, P., and K. N. Liou, 1996: Finite-difference time domain method for light scattering by small ice crystals in three-dimensional space. *J. Opt. Soc. Am. A,* **13**, 2072–2085. doi:10.1364/JOSAA.13.002072.

Zerull, R., R. Giese and K. Weiss, 1977: Scattering measurements of irregular particles vs. Mie theory. *Proc. Soc. Photo-Optical Instrum. Engrs.*, **12**. Instrumentation and Applications: 191–199.

Zerull, R. H., R. H. Giese, S. Schwill and K. Weis, 1980: Scattering by particles of nonspherical shape. In *Light Scattering by Irregularly Shaped Particles*, ed. D. W. Schuerman, 273–282. New York: Plenum.

Zhao, F., 1999: Determination of the complex index of refraction and size distribution of aerosols from polar nephelometer measurement. *Appl. Opt.*, **38**, 2331–2336.